Photochemical & Photobiological Sciences (2023) 22:195–217
https://doi.org/10.1007/s43630-022-00297-x

REVIEWS

Spectroscopic and kinetic characterization of photogenerated charge carriers in photocatalysts

Jenny Schneider[1] · **Mariano Curti**[2]

Received: 16 May 2022 / Accepted: 26 August 2022 / Published online: 8 October 2022

Abstract

The catastrophic consequences of increased power consumption, such as drastically rising CO_2 levels, natural disasters, environmental pollution and dependence on fossil fuels supplied by countries with totalitarian regimes, illustrate the urge to develop sustainable technologies for energy generation. Photocatalysis presents eco-friendly means for fuels production via solar-to-chemical energy conversion. The conversion efficiency of a photocatalyst critically depends on charge carrier processes taking place in the ultrafast time regime. Transient absorption spectroscopy (TAS) serves as a perfect tool to track those processes. The spectral and kinetic characterization of charge carriers is indispensable for the elucidation of photocatalytic mechanisms and for the development of new materials. Hence, in this review, we will first present the basics of TAS and subsequently discuss the procedure required for the interpretation of the transient absorption spectra and transient kinetics. The discussion will include specific examples for charge carrier processes occurring in conventional and plasmonic semiconductors.

Graphical abstract

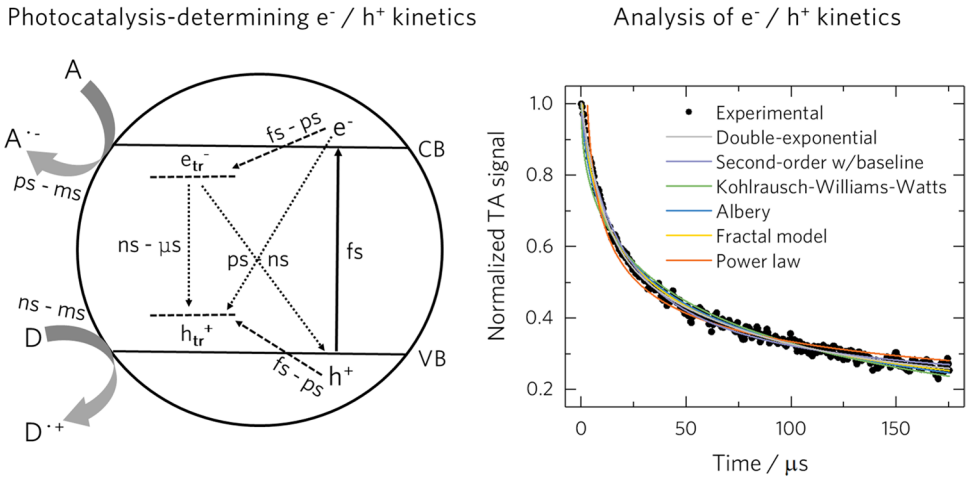

✉ Jenny Schneider
jenny.schneider@lmu.de

✉ Mariano Curti
mcurti@iciq.es

[1] Department of Chemistry, Ludwig-Maximilians-Universität (LMU) München, Butenandtstraße 1-11, 81377 Munich, Germany

[2] Institute of Chemical Research of Catalonia (ICIQ), Barcelona Institute of Science and Technology (BIST), Avda. Països Catalans 16, 43007 Tarragona, Spain

Abbreviations

CB	Conduction band
DFT	Density functional theory
EPR	Electron paramagnetic resonance
GSB	Ground state bleach
KWW	Kohlrausch–Williams–Watts
LUMO	Lowest unoccupied molecular orbital
LSPR	Localized surface plasmon resonance
NIR	Near-infrared

PIA	Photoinduced absorption
PITCT	Plasmon-induced transit charge transfer
RhB	Rhodamine B
SE	Stimulated emission
SP	Surface plasmon
TAS	Transient absorption spectroscopy
TRDRS	Time-resolved diffuse reflectance spectroscopy
VB	Valence band
XPS	X-ray photoelectron spectroscopy
XUV	Extreme ultraviolet

1 Introduction

The first photocatalytic reactions were reported in the second decade of the twentieth century (1910–1920) [1]. The oxidative degradation of organic molecules (e.g. dye and pigments) was observed on the illuminated surfaces of metal oxides, such as zinc oxide, ZnO, and titanium dioxide, TiO_2. Subsequent research focused on the development of photocatalytic materials for the cleaning of surfaces, air, and water. After Honda and Fujishima discovered in 1972, the photosensitizing effect of a TiO_2 electrode for the electrolytic splitting of water, photocatalysis gained additional significance as a potential method to convert solar into chemical energy [2]. In a typical photocatalytic reaction, a photocatalyst is exposed to light, whose energy excites electrons from the filled valence band (VB) to the conduction band (CB). The charge carriers thus generated, that is, the electron in the CB (a reducing species) and the hole in the VB (an oxidizing species), migrate to the surface where they can undergo redox reactions with adsorbed molecules. Herein, the photocatalytic activity represents the ability of a photocatalyst to convert a certain amount of absorbed photons into the respective redox products. Many semiconducting materials show the ability to directly convert light energy into chemical or electrical energy; however, their photocatalytic activity is determined by the character of the photogenerated charge carriers.

Just 12 years after the discovery made by Honda and Fujishima, the active species responsible for TiO_2 photocatalysis, namely electrons and holes, were characterized. Bahnemann et al. [3] reported in 1984 for the first time the spectral identification of the charge carriers formed in colloidal TiO_2 by means of nanosecond transient absorption spectroscopy (TAS, denoted at this time as flash photolysis). Herein, the photocatalyst was excited by a pulsed laser in the nanosecond range resulting in the photogeneration of the electron–hole pairs, which were subsequently monitored through their respective transient optical absorption signature. Nowadays, TAS is a standard characterization method and enables the explanation of material-dependent photocatalytic efficiencies. The decay time or rather the lifetime of the charge carriers varies depending on the morphological and physical properties of the photocatalyst, thus determining its photocatalytic activity.

Transient absorption spectroscopy has significantly advanced over the years, allowing the generation and probing of charge carriers from THz frequencies to hard X-rays in time regimes down to femtosecond time scales and beyond [4]. Several reviews and books provide excellent descriptions of most time-resolved techniques [4–7]. Recently published reviews with a focus on the use of TAS for in situ and operando studies for advanced photoelectrochemical and photocatalytic applications are also available [8–10].

This review is devoted to the interpretation and understanding of the physical properties of charge carriers as observed by time-resolved optical spectroscopy, which still remains an important and frequently far-from-trivial scientific task. The review starts with the basic principle of TAS. The transient absorption features of the electrons and holes photogenerated in organic and inorganic semiconductors are summarized and discussed, followed by the characterization of charge carrier processes in recently developed plasmonic materials. The second part of the review offers a discussion of the mathematical and physical meaning of the transient decay kinetics and its importance for the mechanistic understanding of photocatalytic processes. This overview is intended to be helpful to those working in the field and should stimulate new research activities aiming to elucidate fundamental charge carrier processes occurring in a photocatalyst under illumination, to correlate those processes with the structural and optoelectronic properties and thus to establish a solid platform for the design of novel efficient photocatalysts.

2 Working principle of transient absorption spectroscopy

Transient absorption spectroscopy is a well-established method to study dynamic processes in a wide range of solar energy conversion materials. Time-resolved spectroscopy as we know it today was developed in the 1950s and early 1960s as flash photolysis and relaxation methods, a development that culminated with the Nobel Prize in Chemistry 1967 to Porter, Norrish, and Eigen [11]. The fundamental idea of the method is to use a pulsed excitation source, often denoted as pump source, to excite a sample from the ground to the excited state. The optical absorption of the excited state or other photogenerated intermediates is then spectroscopically monitored by a probe beam at certain time delay after its generation through a second excitation source. In particular, the probe beam intensity before $I_0(\lambda)$ and after the excitation

$I^*(\lambda, \tau)$ of the sample is detected and passed to the transient recorder, oscilloscope, which allows the temporal resolution of the signal (see Fig. 1). Hence, the quantity of interest is ΔA, the difference between the ground state absorption $A_0(\lambda)$ and the excited state absorption $A^*(\lambda, \tau)$.

If the experiment is conducted in transmission mode, ΔA is directly proportional to the concentration c of the photogenerated species in accordance with the Beer-Lambert law:

$$\Delta A = A^*(\lambda, \tau) - A^0(\lambda) = \log\left(\frac{I_0^*}{I^*}\right) - \log\left(\frac{I_0}{I}\right) = log\left(\frac{I}{I^*}\right) = \varepsilon cd, \quad (1)$$

where ε is the extinction coefficient of the formed intermediate, d the beam path length, and $I_0 = I_0^*$.

To obtain quantitative information from TA experiments, it is necessary to measure the extinction coefficients of the species formed in the semiconductor upon excitation. For example, Durrant et al. [12] applied a spectroelectrochemical method to determine the extinction coefficient of the electron and holes in TiO_2.

If the experiments are performed in diffuse reflectance mode (time-resolved diffuse reflectance spectroscopy, TRDRS), then for the quantification of the intermediate's concentrations, several considerations must be taken into account. For an optically dense sample, the reflected light is measured. The reflectance, R, is defined as the quotient of the incident intensity of the analyzing light, $I_0(\lambda)$, and the diffusely reflected light, $J_0(\lambda)$: $R_0(\lambda) = J_0(\lambda)/I_0(\lambda)$. If the laser excitation generates a transient species that has an absorption at wavelength λ, this will result in the decrease of $J_0(\lambda)$ to $J^*(\lambda, \tau)$, while $I_0(\lambda)$ remains constant. Hence,

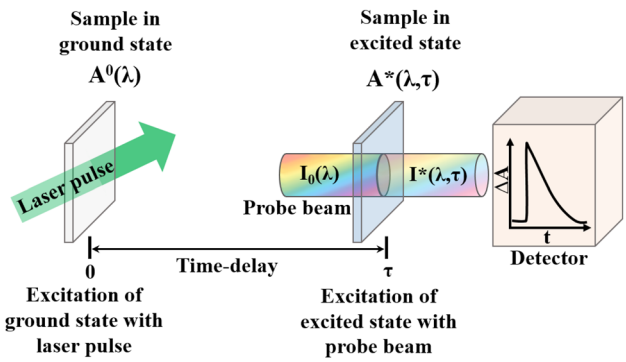

Fig. 1 Principle of transient absorption spectroscopy. Excitation of a sample by a laser pulse leads to the formation of an excited state, the electronic transitions of which are induced by a probe beam and are spectroscopically monitored at a certain time delay after the laser pulse by a detector. Here, the probe beam intensity is measured before $\boldsymbol{I_0(\lambda)}$ and after excitation $\boldsymbol{I^*(\lambda, \tau)}$ and are applied in Eq. (1) to determine $\boldsymbol{\Delta A}$. The transient signal, $\boldsymbol{\Delta A}$, represents the difference between ground state $A^0(\lambda)$ and excited state $A^*(\lambda, \tau)$ absorption

the reflectance will be reduced to $R^*(\lambda, \tau)$. Mathematically, this can be summarized as: [13]:

$$\Delta R = \frac{R_0(\lambda) - R^*(\lambda, \tau)}{R_0(\lambda)} = 1 - R_T^*(\lambda, \tau), \quad (2)$$

where $R_T^*(\lambda, \tau) = R^*(\lambda, \tau)/R_0(\lambda)$. More detailed descriptions of the TRDRS working principle are available elsewhere [3, 13, 14].

In most TRDRS experiments, the concentration of excited states as a function of the distance from the sample surface follows an exponential decay [13]. This is because the experiments are mostly performed at conditions in which the ratio of the number of absorber units to the number of the exciting photons is high; thus, a low conversion percentage of the ground state to the transient state is expected. For the description of the exponentially falling-off concentration, the system can be divided into a series of "thin slices", for which the Kubelka–Munk model is valid. Numerical solutions for this approach predict that a linear relationship exists between the reflectance change $(1 - R_T^*(\lambda, \tau))$ and the total transient species concentration, as long as $(1 - R_T^*(\lambda, \tau))$ remains below 0.1 [15].

Most time-resolved studies on the reaction dynamics of photogenerated charge carriers in semiconductors have been performed in transmission mode, on transparent colloidal dispersions or on transparent films [3, 16–22]. TRDRS allows the observation of the charge carrier dynamics of photocatalyst powders or opaque suspensions [23–25]. A major advantage is that the obtained kinetic data can be directly correlated with the outcome of photocatalytic tests with these samples, since they are used in powdered form in both cases.

Independently from the mode in which the TAS measurements were conducted, the time-resolved absorption changes can be recorded as a function of the probe wavelength. The transient absorption spectra are obtained by plotting ΔA, monitored at a fixed time after the laser pulse excitation, as a function of the wavelength. The obtained transient absorption spectra normally contain three main contributions, the ground state bleach (GSB), stimulated emission (SE) and the so-called photoinduced absorption (PIA) arising from the absorption of the intermediates formed after the excitation, such as the excited states, positive or negative polarons, and trapped states (see Fig. 2).

In transient spectra, GSB appears as a negative band due to the depletion of the ground state occupancy (caused by laser excitation). Accordingly, more light can be transmitted after the sample was excited: $I^*(\lambda, \tau) > I_0(\lambda)$. In luminescent samples, after laser excitation, the probing light can induce the stimulated emission (working principle of lasers) which results in higher light intensity reaching the detector, $I^*(\lambda, \tau) > I_0(\lambda)$, and thus in a negative TA band. PIA is a positive TA signal: here $I^*(\lambda, \tau) < I_0(\lambda)$, since the formed intermediates

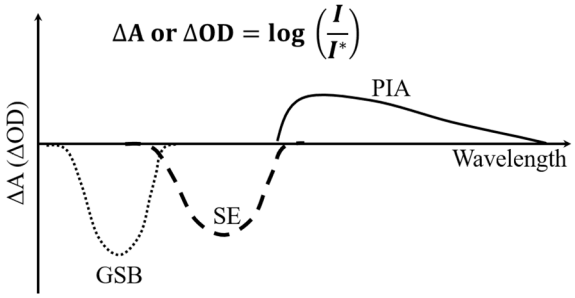

Fig. 2 A plot of Δ*A* vs. wavelength involving three main contributions to the transient absorption spectra

harvest the probing light. PIA bands occur in such systems where successful charge separation has occurred; hence, these are transient bands which are relevant for the discussion of photocatalytic processes. The detailed discussion on the origin of PIA bands reported for organic and inorganic semiconductors will be thus presented in the next section, where we will denote PIA as a transient absorption.

3 Transient absorption spectra of photogenerated electrons and holes

3.1 Conventional organic and inorganic semiconductors

The electrons and holes photogenerated in a semiconductor drive the photocatalytic redox reactions. The spectroscopic tracking of these charge carriers may provide important knowledge to elucidate the photocatalytic reaction mechanisms and to reveal factors influencing the efficiency of the initial steps in photocatalysis. Since the photogenerated charge carriers are transient species, their spectroscopic characterization requires techniques such as TAS. The analysis and interpretation of the electron's and hole's transient absorption spectra are demanding and involve the separation of their transient absorption bands, knowledge of the intermediate's chemical identity, and the assignment of the corresponding electronic transitions.

Under inert atmosphere, both electrons and holes are present after the excitation of the sample, and the recorded TA spectra are typically broad and featureless. The addition of an electron donor or an acceptor enables the separation of the individual wavelength regions where photogenerated electrons and holes absorb. By reacting with electron donors or acceptors, holes or electrons (respectively) are consumed, and thus their contribution to the transient absorption spectra is reduced, in addition to the suppression of undesired recombination reactions.

Alcohols act as perfect electron donors to scavenge photogenerated holes in inorganic semiconductors [26, 27]. For example, Tamaki et al. [27] investigated the reaction dynamics of trapped holes in TiO_2 with different alcohols, and observed a rapid decay of their transient absorption. The lifetime of the trapped holes in methanol, ethanol, and 2-propanol was found to be 300, 1000, and 3000 ps, respectively. Generally, it is assumed that the hole-induced alcohol oxidation includes the cleavage of the C–H bond, resulting in the formation of the respective α-hydroxyalkyl radicals, while the formation of the respective aldehyde occurs in a second step after injection of an electron into the CB of the semiconductor ("current doubling") [28]. For organic polymers used as photocatalysts, alcohols were found to be less active for hole scavenging. Here, basic amines, such as trimethylamine or tri-ethanolamine, are most commonly used as electron donors [29].

Recently, combined experimental and theoretical studies have demonstrated the hole scavenging ability of water [30]. In spherical anatase TiO_2 nanoparticles, water adsorbates trap photogenerated holes. On the contrary, holes formed in faceted TiO_2 are unaffected by the presence of water. The low-coordinated Ti sites, present on nanoparticles, but lacking on faceted surfaces, were found to play a decisive role in water dissociation, which contributes to hole trapping at low-coordinated Ti–OH sites. Hence, water molecules were identified as active species in realistic aqueous operation conditions.

A prominent example of electron scavengers is molecular oxygen, which forms upon reaction with photogenerated electrons a superoxide radical [31, 32]. The reduction of molecular oxygen by electrons trapped in TiO_2 has been reported to occur within less than 100 ns [21], while the reduction process with the free CB electrons occurs 10–100 times slower [32, 33]. These different reaction dynamics can be explained by the fact that the trapped electrons are mostly localized at the surface and thus can be faster transferred to the surface bound oxygen atoms than the bulk located free CB electrons, although the former exhibit a lower reduction potential than the latter. However, to be an efficient electron scavenger, the reaction of the photogenerated electrons with the electron acceptor should be faster than the recombination. Platinum is an alternative electron scavenger, capturing photogenerated electrons within a few picoseconds. A homogeneous deposition of Pt on the semiconductor surface is challenging; typically, there is an unequal distribution of Pt islands [3, 34]. Their formation and optical absorption might affect the transient absorption spectra of the electrons, causing misleading interpretations of the TA results [34]. Silver cations, Ag^+, have also been applied as electron scavengers. Upon reaction with photogenerated electrons, they are reduced to Ag [35, 36]. However, the silver nanoparticles exhibit a strong plasmon absorption at around 430 nm,

i.e., in the wavelength region where photogenerated holes absorb in TiO_2 [34, 37]. Cu^{2+} ions have as well the ability to scavenge electrons, forming Cu^+ ions, which have the advantage that no light is absorbed at wavelengths longer than 350 nm [35].

In addition to the chemical scavenging of charge carriers, the photogenerated electrons or holes can be extracted potentiostatically. Under applied cathodic bias the holes are scavenged, while anodic bias removes the electrons from the system. However, applying a bias to an electrode causes band bending, which might affect the trapping behavior of charge carriers [38]. A recently published review provides a broad overview on the use of transient absorption spectroscopy for in situ and operando studies of photoelectrodes [9].

In summary, it is obvious that there is no optimal scavenger for the photogenerated electrons and holes. For the identification of the spectroscopic regions of electron and holes, a scavenger is indispensable. However, it must always be taken into account that the scavenger might cause chemical or optical changes of the studied material, and thus leads to wrong conclusions [39]. Table 1 summarizes the spectroscopic regions of photogenerated electrons (free or trapped) and holes obtained for various semiconductors in the presence of electron/hole scavengers.

After identifying the spectral region in which electrons and holes absorb, their chemical identity has to be determined to assign the transient absorption spectra to the corresponding transitions. Electron paramagnetic resonance spectroscopy (EPR), an experimental technique to monitor the formation of paramagnetic species, is commonly applied to chemically characterize the electrons and holes in a photocatalyst [90–92]. For example, in TiO_2, the electrons are localized at Ti^{IV} centers converting it to a paramagnetic Ti^{III} species, characterized by g tensor components ranging between 1.9640 and 2.0025. In metal oxides, photogenerated holes are trapped at oxygen centers forming either surface adsorbed $^{\bullet}OH$ radicals or lattice bound $O^{\bullet-}$ radicals. The latter species show a strong EPR signal as well [93]. However, except for a few examples [94], most EPR measurements are conducted at very low temperatures, cooling either with liquid nitrogen or liquid helium. These conditions are very different to the TA experiments, so a direct correlation of the results is sometimes challenging.

Today, with the availability of large-scale facilities specializing in the generation of ultrashort pulses in a wide spectral range, like free electron lasers, or high-power laser facilities, femtosecond pulses can be generated from THz frequencies to hard X-rays [4]. This enables the probing of light–matter interactions over a broad range of time-,

Table 1 Transient absorption band maxima for holes and electrons recorded in the presence of scavengers in different semiconducting materials

Material	TA maxima/nm			Scavengers		References
	h_{tr}^+	e_{tr}^-	e_{CB}^-	e^-donors	e^--acceptor	
TiO_2 (colloidal)	350–550	500–650	–	Polyvinyl alcohol Dichloroacetate SCN^-	Pt	[3, 20, 40–43]
TiO_2 (film)	350, 520/1200	800, 770	< 1000 nm	Methanol	$AgNO_3$	[17, 21, 37, 44–46]
TiO_2 (powder)	430, 470–500	500–770	< 1000 nm	Methanol	Pt, O_2	[23, 47–51]
$Ba_5Ta_4O_{15}$ (powder)	310	650	–	Methanol	–	[26]
WO_3 (film)	430–500	< 750	–	Bias Methanol	$AgNO_3$ Bias	[22, 52–55]
α-Fe_2O_3 (film)	575–650	575	–	Bias	–	[56–63]
ZnO (colloidal/film)	–	700	–	–	N_2O	[64, 65]
Cu_2O (film)	> 475	–	< 850	Na_2SO_3	$AgNO_3$	[66]
$BiVO_4$ (film)	470, 550, 633	–	–	Na_2SO_3 Bias	$AgNO_3$ Fe^{3+}	[36, 67–70]
$BiVO_4$ (powder)	580	–	3435	Methanol NaI	$AgNO_3$	[71–73]
$BiFeO_3$ (film)	–	–	~ 539	–	–	[74, 75]
$SrTiO_3$ (powder/crystal)	500–689	885–909/4000	–	Methanol	O_2	[76–78]
CdS (colloidal)	470–500	300/680	–	NaI Thiophenol	Zwitterionic viologen compound	[79–83]
CdSe (quantum dots)	1300–1938	900–1300/2480	–	1-Octanethiol	1,4-Benzoquinone	[84, 85]
g-C_3N_4 (dispersions)	750	< 700	–	Triethanolamine Methanol, oxalate Bias	Pt $AgNO_3$	[86–89]

energy-, and length-scales. Hence, Baker et al. [95] applied femtosecond extreme ultraviolet (XUV) spectroscopy in conjunction with X-ray photoelectron spectroscopy (XPS) to study ultrafast surface electron dynamics in NiO. XUV spectroscopy probes core-to-valence transitions, which are element-specific and provide detailed electronic structure information, including the transient oxidation state of the Ni metal centers. The findings from this study resolved important questions related to the mechanisms of carrier trapping and subsequent recombination in NiO, and provided parameters for the design of efficient materials.

After the chemical identity of the charge carriers was clarified, the corresponding electronic transitions must be assigned. In general, free electrons are delocalized within the CB [21, 96]. After the absorption of light with certain energies, the free electrons can be excited from a lower state in the CB to a higher state in the CB, known as an interband transition. These transitions are usually observed in the infrared range [21]. The energy levels of the trapped charge carriers are normally located within the band gap [21, 96]. For trapped electrons, their optical transitions correspond to the excitation from the trap state to the CB. For TiO_2, the localized Ti^{3+} electrons undergo d–d transitions upon excitation [97]. The possible transitions of trapped holes are still controversial. Trapped holes represent defect electrons (missing electrons at a certain energy state). In the case of metal oxides, holes correspond to oxygen centered radicals, which could originate either from terminal hydroxyl groups or lattice oxygen [98]. The TA of these radicals can be attributed either to transitions from the trap states to the CB, forming unstable O atoms in the lattice, or from the VB to the trap states. Henderson et al. assumed that the latter transition may not be optically allowed [96]. However, recently published DFT (density functional theory) calculations on TiO_2 demonstrate that the TA of trapped holes is due to the transition of electrons from the VB to trap states [97]. Fig. 3 shows the comparison of experiments and theoretical calculations, with the corresponding electronic transitions responsible for the TA spectra of electrons and holes trapped in TiO_2.

In summary, we can conclude that TAS is an excellent tool to track the short-lived photoactive species. However, it should be considered that the observed transient spectra might be affected by photothermal effects [100] and irreversible changes of the semiconductor caused through laser excitation. For example, Schneider et al. [51, 101] observed irreversible changes of TiO_2 powders induced by the laser excitation in TRDRS, related to the formation of nonreactive trapped electrons accompanied by the release of oxygen atoms from the TiO_2 matrix. The irreversible changes were identified by means of UV–Vis and electron paramagnetic resonance spectroscopies. Moreover, in the case of pure anatase samples, some TiO_2 nanoparticles located in the inner region showed a phase transition to rutile. Furthermore, the laser-induced irreversible changes drastically affected the transient signals. In case of TiO_2, a considerable deceleration of the decay kinetics and a strong increase of the TA signal recorded in the wavelength region where the trapped holes absorb were found. Although for anatase samples, such changes disappear at weak excitation conditions, in the case of rutile, they cannot be avoided.

3.2 Plasmonic semiconductors

With the rapid development of semiconductor-related nanoscience, a new class of low-cost plasmonic semiconducting

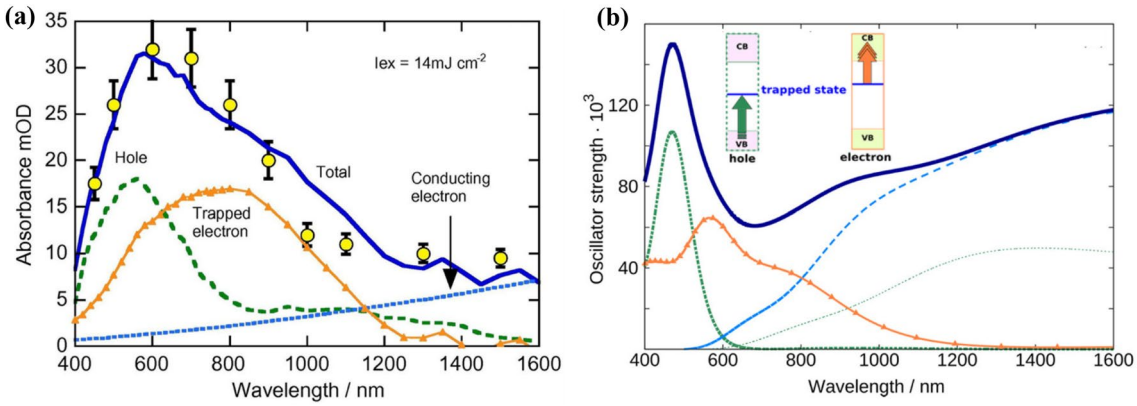

Fig. 3 **a** Experimental transient absorption spectra after high intensity excitation, reprinted from reference [99]. Copyright 2010 Elsevier. **b** Computed absorption spectra of the $(TiO_2)^{38-}$ and $(TiO_2)^{38+}$ clusters, representing an excess electron and excess hole, respectively, in the relaxed $D_{1,e}/D_{1,h}$ (orange solid and green dashed curves) and unrelaxed S_0 geometries (blue dashed and green dotted curves). The solid blue line is the sum of the trapped electron, trapped hole, and CB electron contributions. Inset: Electronic transitions of the trapped holes, from VB to trap state and of the trapped electrons from the trap state to the CB, reprinted from reference [97]. Copyright 2016 American Chemical Society

materials for solar fuel generation has emerged. Plasmonic semiconductors offer new opportunities to overcome some limitations of conventional semiconductors and plasmonic metals. These are heavily doped semiconductors, with a high concentration of free charge carriers. Similar to metals, these free charge carriers can be excited upon illumination, a process known as localized surface plasmon resonance (LSPR). The LSPR phenomenon has been observed in many heavily doped semiconductor nanostructures and quantum dots, including $Cu_{2-x}S$, B-/P-doped Si, $Cu_{2-x}Se$, Sn–In_2O_3, MoO_{3-x}, and Bi_2O_{3-x} [102–108]. Unlike metals, plasmonic semiconductors show broadly tunable plasmon frequencies (from visible to infrared) and rich surface chemistry. Especially, the infrared activity of plasmonic semiconductors is of high interest as it allows to capture an untapped energy source that accounts for 49% of solar irradiation, and thus opens a new avenue for green fuel generation by fully exploiting solar light.

By means of TAS, Zhou et al. [109] demonstrated for the first time plasmon-driven hot electron generation, and transfer from plasmonic metal oxide nanocrystals to surface adsorbed molecules. Here, F and In co-doped CdO nanocrystals were excited with a 1650 nm laser pulse, and the hot electron injection to the adsorbed electron acceptor (Rhodamine B, RhB) was probed in the visible wavelength region (400–700 nm). A strong ground state bleach band matching exactly with RhB absorption, and transient absorption at ~ 412 nm arising from the RhB radical anion, were observed (see Fig. 4a). The analysis of RhB GSB kinetics revealed an electron transfer time of < 50 fs (rise) and 407 fs for a subsequent back electron transfer process (decay). Together with the excitation wavelength- and power-dependent studies, the authors provided a mechanistic picture of the process occurring upon infrared light illumination (Fig. 4c). After photoexcitation, the plasmon resonance damps its energy and excites electrons from the states near Fermi level, E_f, thus depopulating those states in < 10 fs through Landau damping. Subsequent indirect hot electron transfer from the plasmonic semiconductor occurs before electron thermalization. The number of hot electrons above the RhB lowest unoccupied molecular orbital (LUMO) was found to be tunable via the excitation fluence (energy per excited area).

The rich surface chemistry of plasmonic semiconductors enables the coupling not only with molecules as shown in the aforementioned example but also with other photoactive semiconductors. Plasmonic semiconductor nanostructures can be easily assembled onto active supports through a facile wet chemical method. Zhang et al. [110] have fabricated $W_{18}O_{49}$ nanowires (as branches) onto TiO_2 electrospun nanofibers (as backbones). These materials exhibited plasmon enhanced photocatalytic activity for hydrogen generation from ammonia borane upon excitation by low-energy infrared photons. For the elucidation of the photoinduced processes, TAS was performed in combination with theoretical calculations. The 800 nm excitation of pure $W_{18}O_{49}$ resulted in a broad transient absorption band with a maximum at 1045 nm. This transient absorption was assigned to the LSPR, by which free electrons around the Fermi level could reach a virtual high-energy surface plasmon (SP) state to form energetic hot electrons. When $W_{18}O_{49}$ was coupled with TiO_2 to form a branched heterostructure, the transient absorption disappeared. This observation indicated the LSPR-excited hot electron transfer from $W_{18}O_{49}$ branches to the adherent TiO_2 backbones. A thorough kinetic analysis of the transients monitored at various wavelengths confirmed the hot electron transfer process, with fast rate constants of 3.8×10^{12} to 5.5×10^{12} s^{-1}. Such an ultrafast transfer process should hinder the relaxation of hot electrons to low energy levels in plasmonic $W_{18}O_{49}$ and therefore boost the generation of active electrons for executing the catalytic reaction.

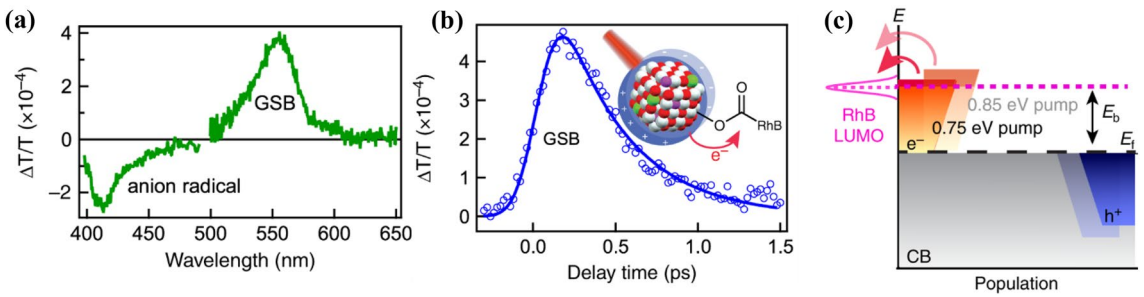

Fig. 4 **a** Transient absorption spectrum of F and In co-doped CdO and RhB showing RhB ground state bleach (GSB) and anion radical induced transient absorption. **b** Transient absorption kinetics of RhB GSB (empty circles) and the exponential fitting (blue line) in F and In co-doped CdO–RhB complex. c) Scheme of hot electron transfer with two excitation energies (0.75 and 0.85 eV) after Landau damping before electron thermalization. The gray region shows the undisturbed filled states in the conduction band. The orange and blue regions represent the excited electrons and empty states left, respectively, after Landau damping under different excitation photon energies. Higher excitation energy leads to more electrons above the barrier height. Reprinted from reference [109]. Copyright 2020 Springer Nature

Among the development of photocatalysts based on the plasmon-induced hot electron transfer, materials conducting plasmon-induced hole transfer were also studied. A novel series of p-type semiconductors such as copper chalcogenide nanocrystals, which show excellent tunable hole-based LSPR absorption in the near-infrared (NIR) region, have attracted much attention as candidates for infrared-responsive photocatalysts [111, 112]. For example, time-resolved infrared spectroscopy enabled the direct observation of hot hole transfer in a LSPR-excited CdS/CuS system [113]. Figure 5a, b show the transient absorption signal obtained for CuS and CdS/CuS upon excitation with 1200 nm laser pulse. The observed bleaches in both systems were attributed to the LSPR bleaching caused through LSPR-excitation-induced sequential events such as hole dephasing, hole–hole scattering, hole–phonon coupling, and lattice heat dissipation. In both systems, a blue shift of the bleaching signals in comparison to the LSPR band occurred. The authors have attributed this phenomenon to the change in the concentration of holes induced either by trapping processes or by hole transfer from CuS to CdS in the heterostructure. A further evidence for the hole transfer from CuS to CdS was a broad and featureless absorption derived from the trapped holes in the CdS phases, detected as a positive signal in the visible region, see Fig. 5b. The kinetic analysis of the bleaching kinetics revealed that hot holes were not directly injected into CdS but instead transferred stepwise via the carrier trapping state. The process was named plasmon-induced transit charge transfer (PITCT). The occurrence of this PITCT process enabled a long-lived charge separation (9.2 µs) with high quantum yields (19%). The PITCT mechanism is summarized in Fig. 5c.

As the aforementioned examples demonstrate, plasmonic photocatalysts exhibit promising potential for enhancing the efficiency and solar light harvesting of important chemical transformations. Transient absorption spectroscopy has served as a perfect tool to elucidate the mechanism of the underlying reaction processes through the analysis of the transient absorption bands and decays. However, the mechanism of plasmonic photocatalysis is still poorly understood and requires more investigation. Especially, the contributions of non-photothermal (i.e., hot carrier) and photothermal pathways remain a question of intense debate [114].

4 Charge carrier kinetics

4.1 Overview

The assignment of TA signals to specific species, as described in Sect. 3, allows extracting important *qualitative* information from a photocatalytic system. As a further step, the analysis of the kinetic profiles provides *quantitative* information on the timescale of the processes. This is generally done by fitting the profiles to a mathematical function that (ideally) captures the main physical characteristics of the system [10, 115]. Thus, the functional form of the profiles already provides physical insights. Moreover, the fitting yields kinetic parameters (e.g., rate constants) that can be used to characterize samples and compare different materials.

When approaching kinetic data, it is important to have in mind the approximate time scale of the different processes. As summarized in Fig. 6 for TiO_2, while excitation is practically instantaneous, charge carrier trapping at the surface (shallow traps) occurs in a few hundred fs, while trapping in the bulk is considerably slower (~ 50 ps) [116]. Recombination starts as soon as 1 ps, and can reach the ns

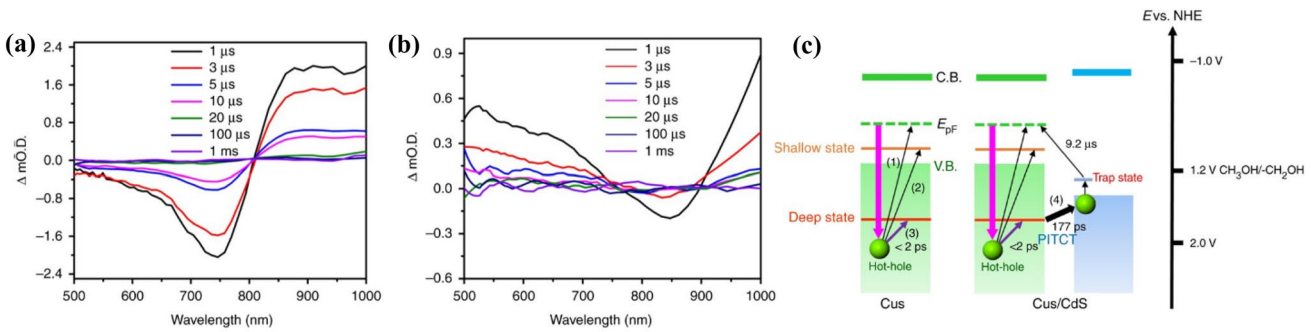

Fig. 5 Time-resolved infrared spectroscopy (TR-IR) spectral changes for CuS (**a**) and CdS/CuS (**b**) nanocrystals from visible to near-infrared regions in the microseconds (µs) time scale. **c** Schematic illustration of the LSPR-induced stepwise hole transfer process. The pink arrows mean plasmon excitation by near-infrared (NIR) light. For CuS NCs, the generated hot holes decayed via hole–hole and phonon–hole scattering (1) or ultrafast hole trapping to the shallow (2) or deep trapping state (3), followed by relaxation to the intrinsic hole state. In CdS/CuS heterostructured nanocrystals, the holes in the deep trapping state transferred to the valence band of the CdS phases (4, PITCT) and the holes in the CdS phases moved to the trapping state, showing structureless absorption in the visible region and recombination to the initial state. PITCT: plasmon-induced transit carrier transfer. Reprinted from reference [113]. Copyright 2018 Springer Nature

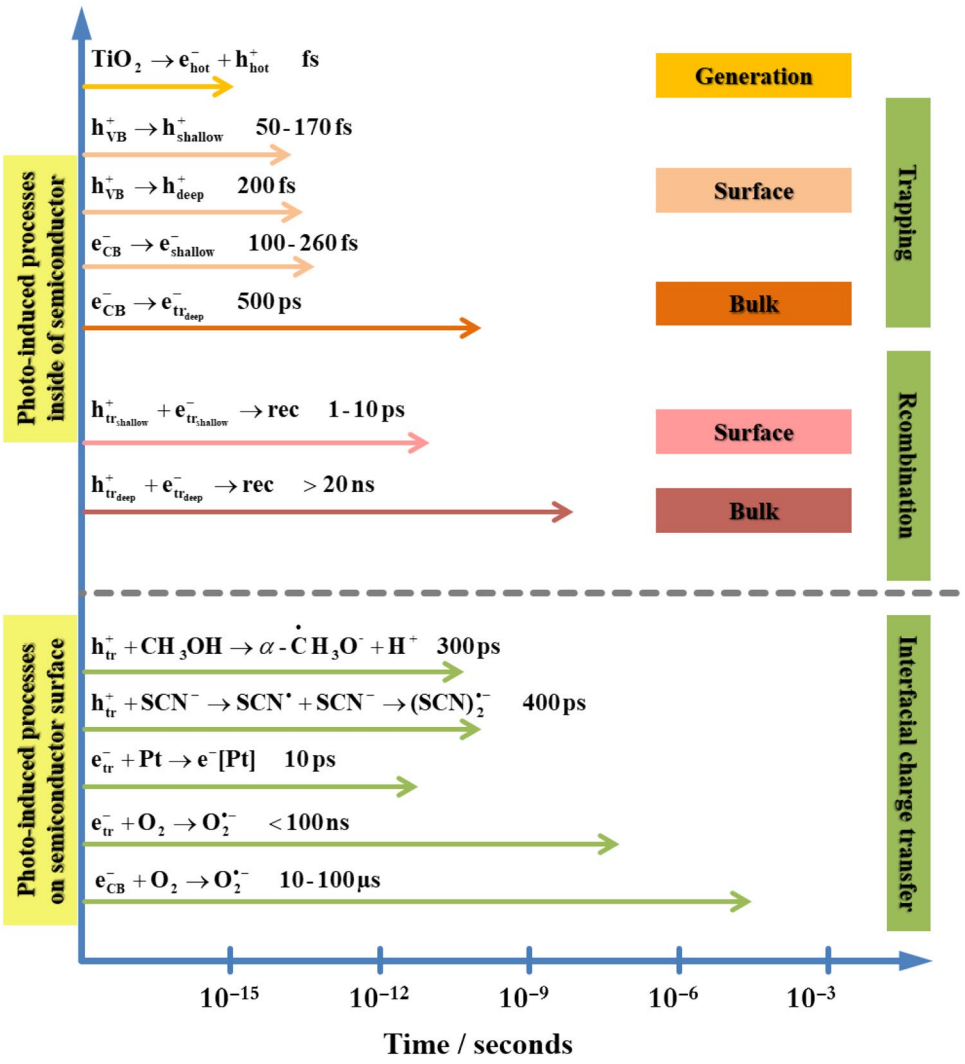

Fig. 6 Scheme of different photoinduced processes observed in transient absorption studies on TiO_2 photocatalysts, and approximate time scales. Adapted with permission from reference [116]. Copyright 2014 American Chemical Society

range for bulk-trapped species. Finally, interfacial charge transfer is strongly dependent on the specific reaction, with e.g., electron transfer to Pt islands occurring in ~ 10 ps, and molecular oxygen reduction occurring in ns to µs time scales. An important consequence is that, except for ultrafast experiments or under strong biases, recombination will most likely be the main observed process, as could be expected from the low quantum yields of photocatalytic reactions (typically below a few percent [117]).

Although the physics of charge carrier dynamics are a complicated subject, a simple picture can provide a good initial overview. Excitation of a photocatalyst, thus, leads to the formation of a bound electron—hole pair: an *exciton*. The high dielectric constant of typical inorganic photocatalysts (e.g., TiO_2) shields their mutual attraction, and thus thermal energy is enough to dissociate the pair in two separate entities, each with a characteristic mobility. Subsequent encounters of the electron and hole results in recombination, which can then be considered as a bimolecular process. From chemical intuition, it can be expected that the kinetics of the process follows a second-order rate law:

$$[c] = \frac{[c]_{t=0}}{[c]_{t=0} k_r t + 1}, \tag{3}$$

where $[c]$ represents the charge carrier (electron or hole) concentration at time t, $[c]_{t=0}$ its concentration at $t = 0$ (i.e., right after excitation), and k_r the second-order rate constant. Indeed, second-order kinetic profiles are commonly observed in TA studies of different photocatalysts [20, 51, 118–120].

This model, however, predicts that the charge carrier concentration reaches zero at long times, in contrast with typical observations. This long-lived absorption has thus been accounted for by including an additional constant term $\varepsilon f \varepsilon$ [120]. This results in a functional behavior termed "second-order with a baseline", that is, possibly, the most widely applied in the analysis of TA decays:

$$[c] = \frac{[c]_{t=0}}{[c]_{t=0}k_r t+1} + f. \quad (4)$$

Illustrating the complexity of recombination processes, it has been observed that the kinetic profiles usually depend on experimental parameters such as the laser pulse intensity or the semiconductor's particle size. These parameters define the average number of photogenerated charge carriers per particle. Serpone et al. [20] analyzed colloidal TiO_2 sols and observed that, when the average number of electron–hole pairs per particle was lower than ~ 0.5, the decays followed first-order kinetics:

$$[c] = [c]_{t=0}e^{-k_r t}. \quad (5)$$

Contrarily, when the average number of pairs per particle was greater than ~ 30, the decays were fitted by the "second-order with a baseline", Eq. (4).

To understand this behavior, it is necessary to recall that the derivation of classical kinetic laws implies that the species of interest are present in numbers large enough to consider their concentrations as continuous variables. In TA experiments, however, the photocatalyst particles act as micro-reactors, where the number of electron–hole pairs is usually much smaller than that limit, thus rendering the basic assumptions of classical kinetic models invalid. The correct treatment then involves stochastic kinetics tools, as was realized by Grätzel and co-workers in 1985 [42]. By assuming a Poisson distribution of electron–hole pairs in colloidal TiO_2 particles, and an exponentially decaying survival probability for single electron–hole pairs, it was possible to obtain an equation that reproduced the charge carrier decays, and correctly reduced to first-order and second-order rate laws under very low or very high initial charge carrier numbers, respectively.

A related stochastic approach was also used to explain the *baseline* behavior (Eq. (4)). Grela and Colussi performed numerical modeling of charge carrier recombination at the surface of colloidal TiO_2 particles, and found that the "baseline" is the consequence of recombination taking place in a 2-dimensional space, i.e., the particles surface [121]. Electron–hole pairs which are initially close together recombine quickly, while those far apart live much longer, giving rise to a phenomenon known as *fractal kinetics*, typical of low-dimensional media [122]. According to this analysis, recombination at the surface never follows second-order kinetics: single electron–hole pairs decay exponentially, while multiple pairs decay in a second-order fashion where the rate constant is actually time-dependent (and thus should be called *rate coefficient*).

Processes in which the rate coefficient k_r are time-dependent are said to follow *dispersive kinetics*, since, equivalently, it can be considered that there is not a unique value for (time-independent) k_r but rather a *distribution* of them [123]. A well-known example is the model of Kohlrausch–Williams–Watts (KWW model) [124, 125]. Although it was initially employed in 1854 by Kohlrausch to describe the discharge of a capacitor [124], it can be applied to chemical reactions with dispersive kinetics, by assuming a Lévy distribution (approximately, an asymmetric Gaussian-like distribution with a 'heavy' tail) for k_r [126]. The KWW function can then be seen as the superposition of many first-order reactions, each with a unique rate constant. The concentration of charge carriers thus follows a so-called *stretched exponential* behavior:

$$[c] = [c]_{t=0}e^{-(k_r t)^{\beta}}, \quad (6)$$

where β represents the distribution width ($0 < \beta \leq 1$). In the $\beta = 1$ limit, the expression reduces to the classical first-order rate law.

A related model is that by Albery and co-workers, initially used to fit interfacial electron transfer kinetics on semiconductor nanoparticles, in which the values of k_r follow a log-normal distribution [127]:

$$[c] \propto \int_0^{\infty} \frac{e^{-(\ln(k_r)-\ln(k_0))^2/\gamma^2}}{k_r} e^{-k_r t} dk_r. \quad (7)$$

Here γ characterizes the distribution width and k_0 is the mean rate coefficient. As γ approaches zero, the dispersion diminishes, and the model approaches a first-order exponential decay.

Sieland et al., while analyzing charge carrier decays in TiO_2 powders, observed that the application of the second-order scheme leads to different kinetic parameters when employing different time windows [128]. To solve this problem, they utilized a fractal kinetic equation that can be understood as a second-order law, modified to account for dispersion in the rate constant [129]:

$$[c] = \frac{[c]_{t=0}(1-h)}{[c]_{t=0}k_r t^{1-h}+(1-h)}, \quad (8)$$

where h ($0 \leq h \leq h$) is the parameter dictating the width of the distribution. By setting $h = 0$ the equation reduces to the classical second-order behavior (Eq. (3)). It is noteworthy that this function has correctly described transient absorption decays of TiO_2 powders spanning the 50 ns to 1 ms time range.

At long times, the right-hand side of the divisor in the fractal model (Eq. (8)) becomes negligible, reducing the expression to a power law dependence [123]:

$$[c] \propto t^{-\alpha}, \quad (9)$$

where α could be associated with $1 - h$ in the previous equation. This model was, for instance, used by Cowan et al. [12] to describe charge carrier decays in the microsecond to second time range in nanocrystalline TiO_2 films under

applied bias. From a physical point of view, the function has been rationalized on the basis of the so-called trapping—detrapping model of charge carrier transport, which, as continuous-time random walk simulations show [130], yields the same kinetic profile. Briefly, the model is based on an energetic distribution of trap states, in which electrons are continuously trapped and later de-trapped with help from thermal energy. The assumption of an exponential density of trap states leads to a power law behavior for the recombination kinetics [130, 131].

In the following, we give a more detailed view and a few applications for each of these models.

4.2 Classical kinetics models

We start with the simplest case, i.e., a first-order reaction representing the decay of a charge carrier c (an electron or a hole), with a rate constant k_r:

$$c \xrightarrow{k_r} \text{(recombination)}. \tag{10}$$

The rate r for a first-order reaction in a homogeneous medium is:

$$r = -\frac{\mathrm{d}[c]}{\mathrm{d}t} = k_r[c]. \tag{11}$$

The derivative here implies that $[c]$ is a real variable, a valid assumption when e.g., dealing with an Avogadro's number of molecules. However, this is not true for photogenerated charge carriers in transient absorption experiments, since laser excitation produces at most a couple hundred per particle. Omitting this issue for the moment, the equation can be integrated to yield the familiar first-order equation, or *exponential decay*:

$$[c] = [c]_{t=0}e^{-k_r t}. \tag{12}$$

From the physical point of view, this simple model could be related to *primary geminate recombination*, that is, before charge carriers migrate on separate paths. This is relevant for semiconductors with a low dielectric constant (e.g., organic), or in low temperature experiments. Exponential decays are also observed in experiments with low average numbers of photogenerated charge carriers [20, 42, 132]. For example, Tamaki et al. [132] analyzed transparent nanocrystalline TiO_2 films at different excitation intensities, and determined that pulses with energies below 160 nJ led to average numbers of photogenerated pairs of one or less per particle (Fig. 7). An important point is that the profiles measured under these conditions fall on top of each other upon normalization, a signature of true mono-exponential decays [10].

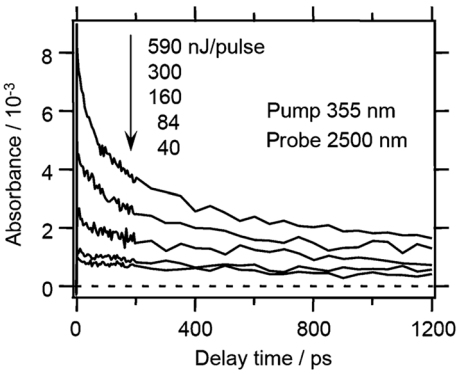

Fig. 7 Transient absorption decays for nanocrystalline TiO_2 films. Excitation was performed at 355 nm and detection at 2500 nm. The intensity of the excitation pulse varied from 590 to 40 nJ pulse^{-1}, from top to bottom. Republished with permission of the Royal Society of Chemistry, from reference [132]; permission conveyed through Copyright Clearance Center, Inc.

When analyzing TA kinetics, it is often found that they can be fitted with a linear combination of exponential decays. This could be the result of *consecutive reactions*. An example is the situation in which charge carriers recombine only in their trapped state:

$$c_{\text{free}} \xrightarrow{k_r} c_{\text{trapped}} \xrightarrow{k_{r,2}} \text{(recombination)}. \tag{13}$$

In this case we have:

$$\frac{\mathrm{d}[c_{\text{free}}]}{\mathrm{d}t} = -k_r[c_{\text{free}}], \tag{14}$$

$$\frac{\mathrm{d}[c_{\text{trapped}}]}{\mathrm{d}t} = k_r[c_{\text{free}}] - k_{r,2}[c_{\text{trapped}}]. \tag{15}$$

Equation (14) is solved in the same way as Eq. (11):

$$[c_{\text{free}}] = [c_{\text{free}}]_{t=0}e^{-k_r t}. \tag{16}$$

For Eq. (15), assuming $[c_{\text{trapped}}]_{t=0} = 0$ and $k_r \neq k_{r,2}$, after some algebra [133] we get:

$$[c_{\text{trapped}}] = \frac{k_r[c_{\text{free}}]_{t=0}}{k_{r,2}-k_r}\left(e^{-k_r t} - e^{-k_{r,2}t}\right). \tag{17}$$

If both c_{free} and c_{trapped} give rise to transient absorption, the observed signal ΔA will be a linear combination of both concentrations (accounting for possibly different absorption coefficients, A and B):

$$\Delta A = A[c_{\text{free}}] + B[c_{\text{trapped}}]. \tag{18}$$

After rearranging and grouping constants together, we get a functional dependence known as *double-exponential* or *biphasic decay*:

$$\Delta A = Ce^{-k_r t} + De^{-k_{r,2} t}. \tag{19}$$

An alternative mechanism that results in a multi-exponential decay originates when similar species decay by different pathways. For instance, we could consider that charge carriers trapped in the surface or in the bulk, while resulting in similar transient absorption spectra, could decay with different rates:

$$c_{\text{surftrapped}} \overset{k_{r,\text{surf}}}{\rightarrow} \text{(recombination)}, \tag{20}$$

$$c_{\text{bulktrapped}} \overset{k_{r,\text{bulk}}}{\rightarrow} \text{(recombination)}. \tag{21}$$

Both species decay exponentially:

$$\left[c_{\text{surftrapped}}\right] = \left[c_{\text{surftrapped}}\right]_{t=0} e^{-k_{r,\text{surf}} t}, \tag{22}$$

$$\left[c_{\text{bulktrapped}}\right] = \left[c_{\text{bulktrapped}}\right]_{t=0} e^{-k_{r,\text{bulk}} t}. \tag{23}$$

If both species present transient absorption, then the total signal will be given by:

$$\Delta A = A\left[c_{\text{surftrapped}}\right] + B\left[c_{\text{bulktrapped}}\right]. \tag{24}$$

Combined with Eqs. (22) and (23), and grouping constants, it again results in a double exponential decay:

$$\Delta A = Ce^{-k_{r,\text{surf}} t} + De^{-k_{r,\text{bulk}} t} \tag{25}$$

This type of behavior has been observed, for instance, by Zhang et al. for colloidal CdS suspensions [134], and by Horikoshi et al. for oxygen-vacancy rich TiO_2 powders [135]. In the latter case, illustrated in Fig. 8, the authors analyzed the decays in the presence or absence of a microwave field. For dry samples, it made no difference, but in wet pastes, recombination significantly slowed down under microwave irradiation. Moreover, the observation of a double-exponential decay was explained in terms of the recombination mechanism: the fast component was attributed to recombination of free or shallowly-trapped electrons with holes, while the slow decay was related to recombination of deeply trapped electrons with (free or trapped) holes [135].

A mechanism that *does not* result in multi-exponential profiles is that of parallel decay channels. For instance, we could assume that charge carriers recombine through two separate pathways (e.g., radiative and non-radiative):

$$c \overset{k_r}{\rightarrow} \text{(recombination)} \quad \text{and} \quad c \overset{k_{r,2}}{\rightarrow} \text{(recombination)} \tag{26}$$

The corresponding differential equation is now:

$$-\frac{\mathrm{d}[c]}{\mathrm{d}t} = k_r[c] + k_{r,2}[c] = (k_r + k_{r,2})[c] = k_r'[c]. \tag{27}$$

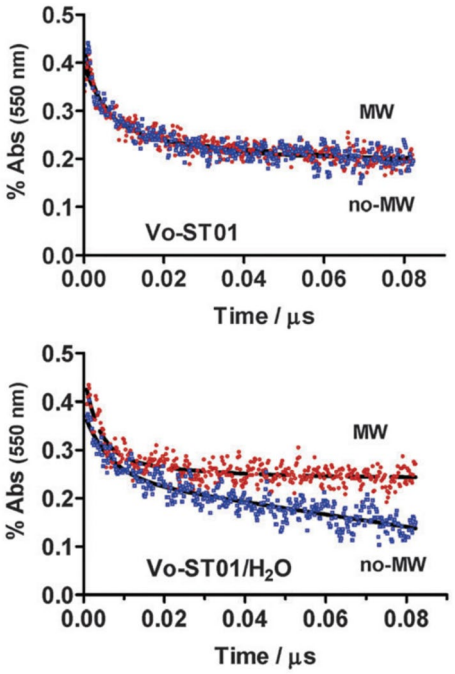

Fig. 8 Transient absorption decays for oxygen-vacancy rich TiO_2 powders, in dry or wet conditions (top and bottom, respectively). Excitation was performed at 532 nm, and detection at 550 nm. Blue and red circles correspond to data points in absence or presence of microwave irradiation, respectively. Lines show double-exponential fittings. The material was prepared by heat-treating commercial TiO_2 in the presence of molecular hydrogen. Republished with permission of the Royal Society of Chemistry, from reference [135]; permission conveyed through Copyright Clearance Center, Inc.

which can then be integrated to obtain a mono-exponential decay, with a rate constant $k_r' = k_r + k_{r,2}$. It is clear then that a parallel decay channel does not change the kinetic profile but only its apparent rate constant.

In cases where the electron—hole pairs dissociate into its components, is perhaps more meaningful to consider a second-order mechanism. In the equal-concentration case, the differential equation reads:

$$\frac{\mathrm{d}[c]}{\mathrm{d}t} = -k_r[c]^2. \tag{28}$$

After rearrangement and integration, we get:

$$[c] = \frac{[c]_{t=0}}{[c]_{t=0} k_r t + 1}. \tag{29}$$

There are many examples of its use from femtosecond to microsecond time windows [20, 51, 118–120]. An important observation is that the derived second-order kinetic constants

for recombination are frequently correlated with the photonic efficiency of photocatalytic processes [26, 49, 136], justifying its wide application despite the simplicity of the physical model.

4.3 Dispersive kinetics models

The previous section deals with classical first-order or second-order mechanisms, with a distinct rate constant for each elementary step. However, in reaction media that are not spatially and energetically homogeneous, the rate constants are not unique but instead follow a distribution. A typical example is the hydrogen abstraction reaction by alkyl radicals in organic glasses [137], which instead of following (pseudo) first-order kinetics, is empirically described by a function termed *stretched exponential* or Kohlrausch–Williams–Watts (KWW) function [124, 125]:

$$[A] = [A]_{t=0} e^{-(k_r t)^{\beta}}, \tag{30}$$

where $0 < \beta \leq 1$. In the $\beta = 1$ limit, the equation is reduced to an exponential decay (Eq. (10)). One way to look at this equation is by assuming that k_r is not a constant but instead changes over time, $k_r = k_r'(t)$. Thus, the exponential factor in the last equation can be rewritten as:

$$-(k_r t)^{\beta} = -{k_r}^{\beta} t^{\beta} = -{k_r}^{\beta} t^{\beta-1} t = -k_r'(t) t. \tag{31}$$

This implies that the reaction follows a first-order equation, where the time-dependent rate *coefficient* $k_r'(t)$ equals ${k_r}^{\beta} t^{\beta-1}$, i.e., the apparent rate constant gets progressively smaller over time.

An alternative interpretation assumes that the rate coefficient is time-independent, and instead of a unique value, there is a distribution of them. In nanocrystalline photocatalysts, this could be caused e.g., by particle polydispersity. Under this view, stretched exponential function can be understood as the summation of mono-exponential decays with different k_r values, representing an ensemble of particles where recombination occurs at distinct rates [126, 138]:

$$[c] \propto e^{-(k_r t)^{\beta}} = \int_0^{\infty} g_{\mathrm{KWW}}(k_r, \beta) e^{-k_r t} \mathrm{d}k_r. \tag{32}$$

Here $g_{\mathrm{KWW}}(k_r, \beta)$ is the probability distribution describing the possible values of k_r and their associated probability. The corresponding function for the KWW model is called a Lévy positive alpha-stable distribution. There are closed-form expressions only for a small set of β values, such as $\beta = 1/2$ [138]. More generally, it can be calculated as [138]:

$$g_{\mathrm{KWW}}(k_r, \beta) = \frac{1}{\pi} \int_0^{\infty} e^{-u^{\beta} \cos(\pi\beta/2)} \cos\left[k_r u - u^{\beta} \sin\left(\frac{\pi\beta}{2}\right)\right] \mathrm{d}u. \tag{33}$$

From a qualitative point of view, the distribution function shows an asymmetric, approximately Gaussian shape, with a 'heavy' tail.

The KWW model was applied, for instance, by Kamat et al. [139] to describe electron injection from CdSe quantum dots to TiO_2 nanoparticles, as observed in femtosecond transient absorption experiments, or by Durrant et al. [32], who studied interfacial electron transfer from TiO_2 films to molecular oxygen in the presence of ethanol (hole scavenger). Another interesting example is that by Castellano et al. [140], who applied time-resolved photoluminescence and transient absorption spectroscopies to pyrenyl-functionalized CdSe quantum dots, and found stretched-exponential decays (with similar kinetics) for both sets of experiments (Fig. 9).

Other rate constant distributions lead to different models. For instance, the one from Albery and co-workers [127] assumes a log-normal distribution of the first-order rate constant. The physical meaning is that instead of a unique activation energy $\Delta G^{\dagger}$ there is a (Gaussian) distribution of them [126]:

$$\Delta G^{\dagger} = \Delta G_0^{\dagger} + \gamma x RT. \tag{34}$$

Here γ determines the width in energy dispersion (with $\gamma = 0$ leading to the first-order case), while the possible values of x follow a Gaussian distribution function ($p(x) \propto e^{-x^2}$). By substituting into the Arrhenius equation, we get [126]:

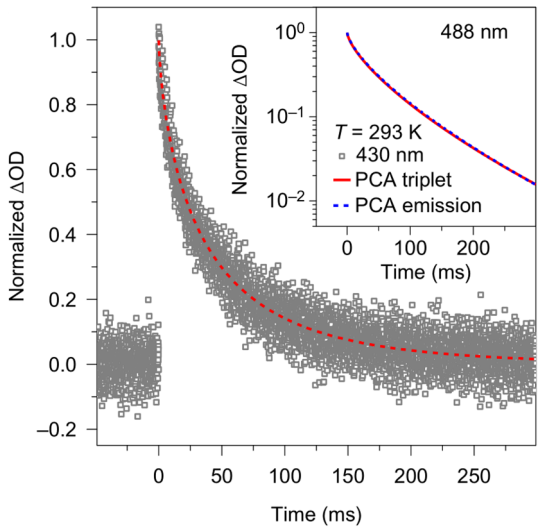

Fig. 9 Transient absorption decay of 2.4 nm CdSe quantum dots functionalized with 1-pyrene-carboxylic acid (PCA). Excitation was performed at 488 nm with a 2 mJ pulse, and detection at 430 nm. The red lines show the fit to a stretched-exponential function. The inset compares the fitted function to that obtained from the fitting of photoluminescence data. Reprinted by permission from Springer Nature: Nature Chemistry, reference [140], Copyright 2017

$$k_r \propto e^{-\frac{\Delta G_0^{\dagger}}{RT}-\gamma x} = k_0 e^{-\gamma x}, \tag{35}$$

where k_0 represents the mean rate constant. The rate law is obtained by summing over all possible values of k_r, or, equivalently, all possible values of x [126]:

$$[c] \propto \int_{-\infty}^{\infty} e^{-x^2} e^{-k_0 t e^{-\gamma x}} \mathrm{d}x. \tag{36}$$

Changing variables, this equation can be expressed in terms of the explicit form of the distribution function $g_{\mathrm{Albery}}(k_r)$, in a similar way as for the KWW model [126]:

$$[c] \propto \int_0^{\infty} g_{\mathrm{Albery}}(k_r) e^{-k_r t} \mathrm{d}k_r. \tag{37}$$

With:

$$g_{\mathrm{Albery}}(k_r) = \frac{e^{-\frac{(\ln(k_r)-\ln(k_0))^2}{\gamma^2}}}{k_r}. \tag{38}$$

The equation shows that k_r follows a log-normal distribution. To fit experimental data, Eq. (36) must be integrated. This can be done using the extended Simpson's rule, resulting in [127]:

$$\frac{[c]}{[c]_{t=0}} = \left(\frac{0.2}{3\pi^{\frac{1}{2}}}\right) \begin{Bmatrix} 2\left[f(0.1)+f(0.3)+f(0.5)+f(0.7)+f(0.9)\right] \\ +f(0.2)+f(0.4)+f(0.6)+f(0.8)+e^{-k_0 t}\end{Bmatrix}, \tag{39}$$

where $f(\lambda) = \lambda^{-1} e^{-(\ln\lambda)^2}(e^{-k_0 t\lambda^{\gamma}} + e^{-k_0 t\lambda^{-\gamma}})$. Both γ and k_0 are used as fitting parameters.

This model was applied, for instance, by Draper and Fox to analyze the transient absorption profiles of photoinduced reactions over aqueous suspensions of TiO_2 powders (particularly, photooxidation reactions) [141, 142]. The distribution in rate constant values was attributed to the dispersion in particle radii. Among other examples [143], the Albery model was also employed by Peek et al. [144] to analyze the emission decay of Cr(VI) ions supported on silica. Interestingly, they found a significant change in the dispersion width values γ when reducing the temperature to 77 K, concluding that at low temperature there is a wider distribution of emitting sites, caused by a larger number of emitting sites.

The Albery and KKW models, as described above, are ultimately based on first-order kinetics. Other models are derived instead from dispersive second-order kinetics. The *fractal model* of Sieland et al. [128] can be understood in these terms by assuming a time-dependent rate coefficient k_r' for the classical second-order expression (Eq. (29)):

$$k_r' = k_r t^{-h}. \tag{40}$$

The equation for the fractal model is thus:

$$[c] = \frac{[c]_{t=0}(1-h)}{[c]_{t=0} k_r t^{1-h} + (1-h)}. \tag{41}$$

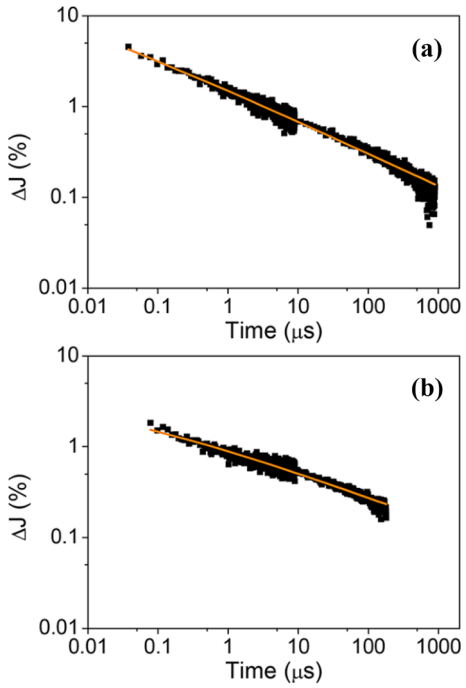

Fig. 10 Transient absorption decays observed at 500 nm for commercial anatase TiO_2 powders (Top: Kronos1001, bottom: PC500). The orange lines show the fits to the fractal model. Excitation was performed at 355 nm. Reprinted with permission from reference [128]. Copyright 2017 American Chemical Society

Similarly to the previous models, h ($0 \le h < 1$) describes the dispersion in the recombination rates, related by the authors to spatial heterogeneity [128]. This model was applied to transient absorption measurements of TiO_2-based powders, performed in reflectance mode on a microsecond time scale (Fig. 10). Although these decays could be fitted with the "second-order with a baseline" classical model, the authors noted that this only worked for short time windows, and the kinetic parameters depended on the chosen windows. This is in line with observations from other authors [145], and was analyzed by Grela and Colussi in their stochastic model [121]. The fractal model, on the contrary, was successfully applied to different time windows and laser excitation energies. Moreover, the calculated k_r values were strongly correlated with the photonic efficiencies for NO degradation over different TiO_2 samples [146], although this correlation was not observed for other photocatalytic reactions (e.g., acetaldehyde degradation).

As described above, the Albery model assumes a Gaussian distribution of activation energies. Alternatively, the assumption of an exponential distribution ($p(x) \propto e^{-x}$, with $x \ge 0$), leads, in analogy with Eq. (37), to [126]:

$$[c] \propto \int_0^{\infty} e^{-x} e^{-k_0 t e^{-\gamma x}} \mathrm{d}x. \tag{42}$$

In the limit $k_0 t \gg 1$, the integral can be solved to get the *power law* time dependence [147]:

$$[c] \propto t^{-\alpha}. \tag{43}$$

With $\alpha = 1/\gamma$ and $0 < \alpha \leq 1$ determining the width in energy dispersion. In the same way as for the KWW and Albery models, the power law decay can be interpreted as a superposition of first-order processes with unique rate constants [126]:

$$[c] \propto t^{-\alpha} = \int_0^\infty g_{\text{Power Law}}(k_r) e^{-k_r t} \mathrm{d}k_r. \tag{44}$$

With:

$$g_{\text{Power Law}}(k_r) = \Gamma(\alpha)^{-1} \left(\frac{k_r}{k_0}\right)^{\alpha-1}, \tag{45}$$

where Γ is the gamma function. An interesting observation is that, at long times, the fractal model (Eq. (41)) reduces to a power law time dependence for $[c]$.

Cowan et al. observed [12] power law decays on TA measurements of nanocrystalline TiO_2 electrodes under applied potentials. By means of the bias, the authors manipulated holes lifetimes; without bias, recombination was the main process, and it followed power law kinetics. However, at positive potentials the lifetime of holes was long enough for water oxidation to compete with recombination. Under these conditions, fittings were only successful when adding a second decay component given by a stretched exponential function (Eq. (30)), and related to the consumption of holes by the water oxidation reaction.

4.4 Stochastic models

In both classical and dispersive kinetic models, an underlying assumption is that charge carrier concentration $[c]$ is a continuous real-valued function of time. However, in nanocrystalline materials, each particle acts as a microreactor where the number of photogenerated charge carriers is at most a couple hundred, and thus $[c]$ is integer-valued. As an example, if 10 electron–hole pairs were generated in 100 particles, the classical view would wrongly assume that all particles would be populated with 0.1 pairs. The correct description of 90% empty particles and 10% particles with one electron–hole pair (neglecting the small number of particles populated with two or more pairs) thus calls for stochastic kinetics to be employed.

Indeed, Rothenberger et al. [42] derived a stochastic rate equation from simple assumptions, the most important being that the survival probability of a single electron–hole pair decreases exponentially with time, and that the initial distribution of pairs follows Poisson statistics. Using this expression, the authors successfully described the kinetic profiles, including the limiting cases of very low and very high initial occupancies, which result in first-order and second-order behaviors, respectively. These approximations were determined to be valid for an average number of pairs lower than 0.5 and larger than 30 per particle, respectively.

Another good example of stochastic treatments is that by Grela and Colussi, who performed numerical modeling of electron–hole recombination (and reactive processes) on the surface of colloidal TiO_2 particles [121]. In this simple but elegant model, the surface is modeled as a square 2D periodic lattice, and electron and holes are initially generated at random positions. Moreover, holes perform a random walk on the surface, while electrons are fixed (thus assuming that they are deeply trapped in colloidal TiO_2). Under these conditions, recombination in particles with multiple pairs follows dispersive second-order kinetics, with the rate coefficient approaching a $t^{-1/2}$ dependence. This behavior is explained by the inhomogeneity in the initial distribution of charge carriers on the surface: while electron and hole pairs generated at close positions promptly recombine, those farther apart survive for longer times. Electron–hole pairs with very long lifetimes are then responsible for the "baseline" behavior previously mentioned (Eq. (4)). Under low average numbers of photogenerated electron–hole per particle, the simulations correctly reproduce the experimentally observed [42] mono-exponential decays.

A remarkable success of this work is that, using a *single set* of kinetic parameters, it can correctly fit transient absorption decays for TiO_2 colloids of different sizes, in the presence or absence of molecular oxygen, and at low and high laser irradiances. On the other hand, the model is built on assumptions (mobile holes, immobile electrons) that may be valid only for colloids, and not, for instance, for powders such as Evonik P25 TiO_2, where electrons freely diffuse [148].

Related models based on charge carriers random walk were also developed, by Nelson and others [130, 131, 149, 150], to understand recombination processes in dye-sensitized solar cells. They pay special attention to electron traps, as they have been observed to reduce electronic conductivity by several orders of magnitude [149]. The specific charge transport model is indeed central to these methods. In the trapping–detrapping model [150], electrons are assumed to move through delocalized states in the CB, sporadically getting trapped and subsequently released by thermal fluctuations. In both rutile and anatase TiO_2, the charge of photogenerated electrons produces a distortion of the lattice that leads to *self-trapping* at Ti^{IV} sites (also called small polaron formation) [151–153]. There is thus a potential energy barrier for electron migration to another Ti^{IV} site. Random walk simulations employing this model and an exponential distribution of

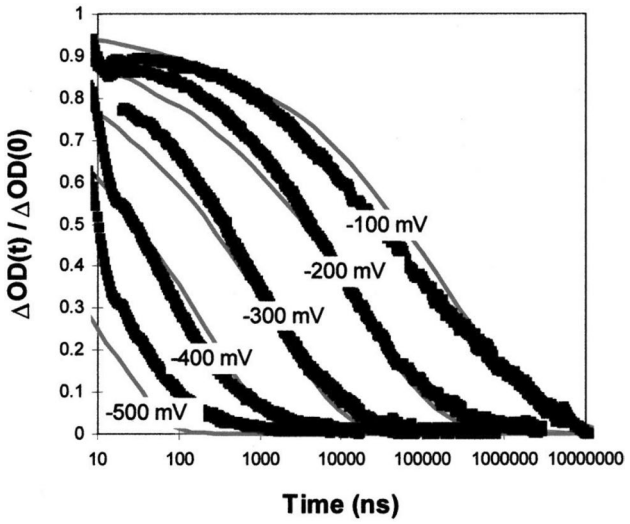

Fig. 11 Normalized transient absorption decays for TiO_2 electrodes under different applied electrical potentials. Black dots show experimental data and gray lines are the results of continuous-time random walk simulations. Reprinted figure with permission from reference [130]. Copyright 2001 by the American Physical Society

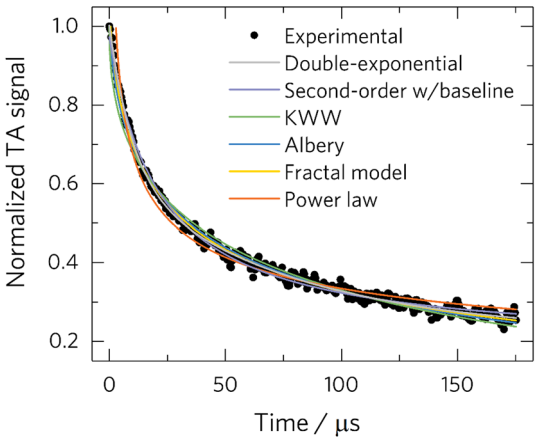

Fig. 12 Transient absorption decay at 500 nm for a Millennium PC105 anatase TiO_2 powder (circles), together with fittings to six different kinetic models (colored lines). Excitation was performed at 355 nm and at a 5.1 mJ cm^{-2} intensity, and detection was done in reflectance mode

trap states nicely result in power law kinetics for recombination (Eq. (43)) [130], thus providing a physical basis for the application of this model. In addition, they can explain the strong dependence of the recombination rate in dye-sensitized systems on the applied bias, and have in some cases shown a remarkable agreement with experimental data using just one fitting parameter (Fig. 11) [130].

4.5 Practical considerations

From the above discussion, it may be concluded that the proper description of charge carrier kinetics requires a stochastic analysis. However, the development and application of such models is a big task on itself, and thus it is often outside the scope of TAS investigations. Moreover, fitting experimental data with these models is not straightforward, complicating the analysis. On the other hand, fitting to either classical or dispersive kinetic schemes tends to be much easier, and thus these models are more widespread, even while they are not physically as sound as stochastic ones.

Looking at their functional form, these different kinetic models may seem unrelated to each other. However, as described above, they are closely interrelated. Employing classical kinetics, and depending on the specific mechanism, mono-, multi-exponential, and second-order decays can be easily obtained (e.g., Equations (11), (18), and (28)). The "second-order with a baseline" function (Eq. (4)) is simply an empirical correction on the latter. As a step further in complexity, dispersive kinetic schemes are based on two alternative interpretations: the rate coefficient is time-dependent, or equivalently, it is constant but there is a distribution on its values. Thus, a superposition of first-order decays in which the rate constant follows a Lévy distribution leads to the KWW model. If the rate constants follows instead a log-normal distribution, we obtain the Albery model. The assumption of a distribution in the rate constants for a second-order decay leads to the fractal model. This model, in turn, is reduced to a power law decay at long times.

Depending on the system and processes of interest, any of these models could result in an adequate fitting to the experimental data. However, as in any reaction kinetics problem, a good fit to a specific model does not allow to establish a mechanism. Often, kinetic schemes with different physical justifications result in similar functional forms [154], a problem exacerbated by the often noisy profiles obtained from TA. To illustrate this point, in Fig. 12, we show the transient absorption decay of a commercial TiO_2 photocatalyst powder; six different models yield a satisfactory fitting. In other situations, the simultaneous occurrence of multiple processes requires the combination of several models to adequately describe the kinetic profiles [12].

Transient absorption spectroscopy is often used as a characterization tool in sets of photocatalytic materials, where correlations are sought between, e.g., decay lifetimes and photocatalytic rates. Therefore, if a particular model adequately describes the kinetics of the entire series, its application may be useful to obtain kinetic parameters and correlate with reactions rates, even though the physical basis of the model may not be clear. Nevertheless, in this case, it may be worth considering the use of a more transparent parameter, such as the time needed for the transient signal

to reach 50% of its initial value [57, 155]. The same metric can be used in situations where the kinetic profiles are not easily described by these models, such as in the presence of electron donors or acceptors [156].

A prerequisite to apply these kinetic models is information on the spectral signatures on the charge carriers of interest (Sect. 3.1). TA signals are thus typically analyzed at a wavelength where contributions are mainly related to a specific species. Alternatively, an interesting approach that combines signal assignment and kinetic modeling is the so-called *global target analysis* [157]. Briefly, the full spectral data ("global") are fitted as a function of time, on the basis of a pre-established kinetic model ("target"). Although not commonly employed for photocatalytic systems, there are some recent interesting examples, such as the ultrafast studies on graphitic carbon nitrides by Corp and Schlenker [87] or the work of Larsen et al. on CdSe/CdS core/shell quantum dots [158].

5 Conclusion

In this review, we have provided an overview of the application of the transient absorption spectroscopy to characterize charge carrier processes in various semiconductor nanomaterials serving a photocatalyst or photoelectrode. The analysis of photocatalysts by TAS starts with the assignment of the transient spectrum features to photogenerated electrons and holes. The main strategy to differentiate their contributions is to employ scavenger compounds that selectively react either with electrons or holes. For instance, the observed transient spectrum in presence of a hole scavenger can be attributed to photogenerated electrons. It is important to bear in mind, however, that the presence of the scavenger will most likely have a strong influence on the physicochemical and optical properties of the studied system. In general, there are no "innocuous" scavengers, and one should consider how the chosen scavenger may affect the system beyond their main function. As an alternative to chemical scavengers, if the semiconductor is configured as an electrode, it is also possible to apply bias to selectively remove charge carriers. For deeper characterization of the charge carriers, analysis with additional methods is required, such as EPR or TAS with advanced spectroscopic resolution.

The analysis of charge carrier kinetic profiles commonly entails the fitting of experimental data with an appropriate function. It is important to bear in mind that, in chemical kinetics, a good fit to a model cannot exclude the occurrence of other, perhaps more complex ones. In a best-case scenario, the strongest conclusion that could be reached is that the chosen model is *adequate* to describe the data. It is also important to recognize that, not rarely, kinetic schemes with different physical justifications can result in similar or even indistinguishable functional shapes. This problem may be exacerbated by the rather noisy profiles normally obtained in TA experiments.

The interpretation of the TAS data presented in this review should be helpful to characterize the reaction dynamics of charge carriers photogenerated in different photocatalysts, and thus to understand the properties of different photocatalytic systems and to specifically develop new photocatalysts with higher activities, longer charge carrier lifetimes or other improved properties.

Funding Open Access funding enabled and organized by Projekt DEAL. The funding was provided by Fakultät für Chemie und Pharmazie, Ludwig-Maximilians-Universität München.

Declarations

Conflict of interest The corresponding authors state that there is no conflict of interest.

References

1. Serpone, N., Emeline, A. V., Horikoshi, S., Kuznetsov, V. N., & Ryabchuk, V. K. (2012). On the genesis of heterogeneous photocatalysis: A brief historical perspective in the period 1910 to the mid-1980s. *Photochemical and Photobiological Sciences, 11*, 1121–1150. https://doi.org/10.1039/C2PP25026H
2. Fujishima, A., & Honda, K. (1972). Electrochemical photolysis of water at a semiconductor electrode. *Nature, 238*, 37–38. https://doi.org/10.1038/238037a0
3. Bahnemann, D., Henglein, A., Lilie, J., & Spanhel, L. (1984). Flash photolysis observation of the absorption spectra of trapped positive holes and electrons in colloidal titanium dioxide. *Journal of Physical Chemistry, 88*, 709–711. https://doi.org/10.1021/j150648a018
4. Ponseca, C. S., Chábera, P., Uhlig, J., Persson, P., & Sundström, V. (2017). Ultrafast electron dynamics in solar energy conversion. *Chemical Reviews, 117*, 10940–11024. https://doi.org/10.1021/acs.chemrev.6b00807
5. Simon, J. D. (1994). Ultrafast dynamics of chemical systems. In Simon, J. D. (Ed.). Springer Netherlands. https://doi.org/10.1007/978-94-011-0916-1. (**ISBN: 978-94-010-4395-3**).
6. Shah, J. (1996). Ultrafast spectroscopy of semiconductors and semiconductor nanostructures. *Springer series in solid-state sciences.* (Vol. 115). Springer. https://doi.org/10.1007/978-3-662-03299-2 ISBN: 978-3-662-03301-2.

7. Luo, C., Ren, X., Dai, Z., Zhang, Y., Qi, X., & Pan, C. (2017). Present perspectives of advanced characterization techniques in TiO_2-based photocatalysts. *ACS Applied Materials and Interfaces, 9*, 23265–23286. https://doi.org/10.1021/acsami.7b00496
8. Lai, T.-H., Katsumata, K., & Hsu, Y.-J. (2021). In situ charge carrier dynamics of semiconductor nanostructures for advanced photoelectrochemical and photocatalytic applications. *Nanophotonics, 10*, 777–795. https://doi.org/10.1515/nanoph-2020-0472
9. Forster, M., Cheung, D. W. F., Gardner, A. M., & Cowan, A. J. (2020). Potential and pitfalls: On the use of transient absorption spectroscopy for in situ and operando studies of photoelectrodes. *The Journal of Chemical Physics, 153*, 150901. https://doi.org/10.1063/5.0022138
10. Miao, T. J., & Tang, J. (2020). Characterization of charge carrier behavior in photocatalysis using transient absorption spectroscopy. *The Journal of Chemical Physics, 152*, 194201. https://doi.org/10.1063/5.0008537
11. Van Houten, J. (2002). A century of chemical dynamics traced through the nobel prizes. 1967: Eigen, Norrish, and Porter. *Journal of Chemical Education, 79*, 548. https://doi.org/10.1021/ed079p548
12. Cowan, A. J., Tang, J., Leng, W., Durrant, J. R., & Klug, D. R. (2010). Water splitting by nanocrystalline TiO_2 in a complete photoelectrochemical cell exhibits efficiencies limited by charge recombination. *Journal of Physical Chemistry C, 114*, 4208–4214. https://doi.org/10.1021/jp909993w
13. Willsher, C. J. (1985). The study of transient absorptions in optically dense materials by diffuse reflectance laser flash photolysis. *Journal of Photochemistry, 28*, 229–236. https://doi.org/10.1016/0047-2670(85)87034-9
14. Wilkinson, F., & Willsher, C. J. (1987). The use of diffuse reflectance laser flash photolysis to study primary photoprocesses in anisotropic media. *Tetrahedron, 43*, 1197–1209. https://doi.org/10.1016/S0040-4020(01)90243-1
15. Lin, T.-P., & Kan, H. K. A. (1970). Calculation of reflectance of a light diffuser with nonuniform absorption. *Journal of the Optical Society of America, 60*, 1252–1256. https://doi.org/10.1364/JOSA.60.001252
16. Shkrob, I. A., Sauer, M. C., & Gosztola, D. (2004). Efficient, rapid photooxidation of chemisorbed polyhydroxyl alcohols and carbohydrates by TiO_2 nanoparticles in an aqueous solution. *The Journal of Physical Chemistry B, 108*, 12512–12517. https://doi.org/10.1021/jp0477351
17. Tamaki, Y., Hara, K., Katoh, R., Tachiya, M., & Furube, A. (2009). Femtosecond visible-to-IR spectroscopy of TiO_2 nanocrystalline films: Elucidation of the electron mobility before deep trapping. *Journal of Physical Chemistry C, 113*, 11741–11746. https://doi.org/10.1021/jp901833j
18. Le Formal, F., Pastor, E., Tilley, S. D., Mesa, C. A., Pendlebury, S. R., Grätzel, M., & Durrant, J. R. (2015). Rate law analysis of water oxidation on a hematite surface. *Journal of the American Chemical Society, 137*, 6629–6637. https://doi.org/10.1021/jacs.5b02576
19. Hagfeldt, A., & Graetzel, M. (1995). Light-induced redox reactions in nanocrystalline systems. *Chemical Reviews, 95*, 49–68. https://doi.org/10.1021/cr00033a003
20. Serpone, N., Lawless, D., Khairutdinov, R., & Pelizzetti, E. (1995). Subnanosecond relaxation dynamics in TiO_2 colloidal sols (particle sizes Rp = 1.0–13.4 Nm) relevance to heterogeneous photocatalysis. *The Journal of Physical Chemistry B, 99*, 16655–16661. https://doi.org/10.1021/j100045a027
21. Yoshihara, T., Katoh, R., Furube, A., Tamaki, Y., Murai, M., Hara, K., Murata, S., Arakawa, H., & Tachiya, M. (2004). Identification of reactive species in photoexcited nanocrystalline TiO_2 films by wide-wavelength-range (400–2500 nm) transient absorption spectroscopy. *The Journal of Physical Chemistry B, 108*, 3817–3823. https://doi.org/10.1021/jp031305d
22. Cristino, V., Marinello, S., Molinari, A., Caramori, S., Carli, S., Boaretto, R., Argazzi, R., Meda, L., & Bignozzi, C. A. (2016). Some aspects of the charge transfer dynamics in nanostructured WO_3 Films. *J. Mater. Chem. A, 4*, 2995–3006. https://doi.org/10.1039/c5ta06887h
23. Yamakata, A., Vequizo, J. J. M., & Matsunaga, H. (2015). Distinctive behavior of photogenerated electrons and holes in Anatase and Rutile TiO_2 powders. *Journal of Physical Chemistry C, 119*, 24538–24545. https://doi.org/10.1021/acs.jpcc.5b09236
24. Kato, K., & Yamakata, A. (2020). Defect-induced acceleration and deceleration of photocarrier recombination in $SrTiO_3$ powders. *Journal of Physical Chemistry C, 124*, 11057–11063. https://doi.org/10.1021/acs.jpcc.0c03369
25. Ichihara, F., Sieland, F., Pang, H., Philo, D., Duong, A.-T., Chang, K., Kako, T., Bahnemann, D. W., & Ye, J. (2020). Photogenerated charge carriers dynamics on La- and/or Cr-doped $SrTiO_3$ nanoparticles studied by transient absorption spectroscopy. *Journal of Physical Chemistry C, 124*, 1292–1302. https://doi.org/10.1021/acs.jpcc.9b09324
26. Schneider, J., Nikitin, K., Wark, M., Bahnemann, D. W., & Marschall, R. (2016). Improved charge carrier separation in barium tantalate composites investigated by laser flash photolysis. *Physical Chemistry Chemical Physics: PCCP, 18*, 10719–10726. https://doi.org/10.1039/c5cp07115a
27. Tamaki, Y., Furube, A., Murai, M., Hara, K., Katoh, R., & Tachiya, M. (2006). Direct observation of reactive trapped holes in TiO_2 undergoing photocatalytic oxidation of adsorbed alcohols: Evaluation of the reaction rates and yields. *Journal of the American Chemical Society, 128*, 416–417. https://doi.org/10.1021/ja055866p
28. Hykaway, N., Sears, W. M., Morisaki, H., & Morrison, S. R. (1986). Current-doubling reactions on titanium dioxide photoanodes. *Journal of Physical Chemistry, 90*, 6663–6667. https://doi.org/10.1021/j100283a014
29. Sachs, M., Sprick, R. S., Pearce, D., Hillman, S. A. J., Monti, A., Guilbert, A. A. Y., Brownbill, N. J., Dimitrov, S., Shi, X., Blanc, F., et al. (2018). Understanding structure–activity relationships in linear polymer photocatalysts for hydrogen evolution. *Nature Communications, 9*, 4968. https://doi.org/10.1038/s41467-018-07420-6
30. Shirai, K., Fazio, G., Sugimoto, T., Selli, D., Ferraro, L., Watanabe, K., Haruta, M., Ohtani, B., Kurata, H., Di Valentin, C., et al. (2018). Water-assisted hole trapping at the highly curved surface of nano-TiO_2 photocatalyst. *Journal of the American Chemical Society, 140*, 1415–1422. https://doi.org/10.1021/jacs.7b11061
31. Memming, R. (1994). In J. Mattay (Ed.), *Electron transfer I. Topics in current chemistry* (Vol. 169, pp. 105–181). Springer. https://doi.org/10.1007/3-540-57565-0_75 ISBN: 978-3-540-57565-8.
32. Peiró, A. M., Colombo, C., Doyle, G., Nelson, J., Mills, A., & Durrant, J. R. (2006). Photochemical reduction of oxygen adsorbed to nanocrystalline tio_2 films: A transient absorption and oxygen scavenging study of different TiO_2 preparations. *The Journal of Physical Chemistry B, 110*, 23255–23263. https://doi.org/10.1021/jp064591c
33. Yamakata, A., Ishibashi, T., & Onishi, H. (2001). Water- and oxygen-induced decay kinetics of photogenerated electrons in TiO_2 and Pt/TiO_2: A time-resolved infrared absorption study. *The Journal of Physical Chemistry B, 105*, 7258–7262. https://doi.org/10.1021/jp010802w
34. O'Rourke, C., Wells, N., & Mills, A. (2018). Photodeposition of metals from inks and their application in photocatalysis. *Catalysis Today*. https://doi.org/10.1016/j.cattod.2018.09.006

35. Friedmann, D., Hansing, H., & Bahnemann, D. (2007). Primary processes during the photodeposition of Ag clusters on TiO_2 nanoparticles. *Zeitschrift für Physikalische Chemie, 221*, 329–348. https://doi.org/10.1524/zpch.2007.221.3.329
36. Ma, Y., Pendlebury, S. R., Reynal, A., Le Formal, F., & Durrant, J. R. (2014). Dynamics of photogenerated holes in undoped $BiVO_4$ photoanodes for solar water oxidation. *Chemical Science, 5*, 2964–2973. https://doi.org/10.1039/C4SC00469H
37. Wang, X., Kafizas, A., Li, X., Moniz, S. J. A. A., Reardon, P. J. T. T., Tang, J., Parkin, I. P., & Durrant, J. R. (2015). Transient absorption spectroscopy of anatase and rutile: The impact of morphology and phase on photocatalytic activity. *Journal of Physical Chemistry C, 119*, 10439–10447. https://doi.org/10.1021/acs.jpcc.5b01858
38. Kisch, H. (2015). *Semiconductor photocatalysis: Principles and applications* (1st ed.). Wiley-VCH. ISBN: 978-3-527-33553-4.
39. Schneider, J., & Bahnemann, D. W. (2013). Undesired role of sacrificial reagents in photocatalysis. *Journal of Physical Chemistry Letters, 4*, 3479–3483. https://doi.org/10.1021/jz4018199
40. Bahnemann, D. W., Hilgendorff, M., & Memming, R. (1997). Charge carrier dynamics at TiO_2 particles: Reactivity of free and trapped holes. *The Journal of Physical Chemistry B, 101*, 4265–4275. https://doi.org/10.1021/jp9639915
41. Shkrob, I. A., & Sauer, M. C. (2004). Hole scavenging and photo-stimulated recombination of electron−hole pairs in aqueous TiO_2 nanoparticles. *The Journal of Physical Chemistry B, 108*, 12497–12511. https://doi.org/10.1021/jp047736t
42. Rothenberger, G., Moser, J., Graetzel, M., Serpone, N., & Sharma, D. K. (1985). Charge carrier trapping and recombination dynamics in small semiconductor particles. *Journal of the American Chemical Society, 107*, 8054–8059. https://doi.org/10.1021/ja00312a043
43. Yang, X., & Tamai, N. (2001). How fast is interfacial hole transfer? In situ monitoring of carrier dynamics in anatase tio_2 nanoparticles by femtosecond laser spectroscopy. *Physical Chemistry Chemical Physics: PCCP, 3*, 3393–3398. https://doi.org/10.1039/B101721G
44. Yoshihara, T., Tamaki, Y., Furube, A., Murai, M., Hara, K., & Katoh, R. (2007). Effect of pH on absorption spectra of photogenerated holes in nanocrystalline TiO_2 films. *Chemical Physics Letters, 438*, 268–273. https://doi.org/10.1016/j.cplett.2007.03.017
45. Tamaki, Y., Furube, A., Katoh, R., Murai, M., Hara, K., Arakawa, H., & Tachiya, M. (2006). Trapping dynamics of electrons and holes in a nanocrystalline TiO_2 film revealed by femtosecond visible/near-infrared transient absorption spectroscopy. *Comptes Rendus Chim., 9*, 268–274. https://doi.org/10.1016/j.crci.2005.05.018
46. Zhu, M., Mi, Y., Zhu, G., Li, D., Wang, Y., & Weng, Y. (2013). Determination of midgap state energy levels of an anatase TiO_2 nanocrystal film by nanosecond transient infrared absorption—excitation energy scanning spectra. *Journal of Physical Chemistry C, 117*, 18863–18869. https://doi.org/10.1021/jp405968f
47. Murakami, Y., Nishino, J., Mesaki, T., & Nosaka, Y. (2011). Femtosecond diffuse-reflectance spectroscopy of femtosecond diffuse-reflectance spectroscopy of various commercially available TiO_2 powders. *Spectroscopy Letters, 44*, 88–94. https://doi.org/10.1080/00387011003699683
48. Colombo, D. P., & Bowman, R. M. (1996). Does interfacial charge transfer compete with charge carrier recombination? A femtosecond diffuse reflectance investigation of TiO_2 nanoparticles. *Journal of Physical Chemistry, 100*, 18445–18449. https://doi.org/10.1021/jp9610628
49. Furube, A., Asahi, T., Masuhara, H., Yamashita, H., & Anpo, M. (1999). Charge carrier dynamics of standard TiO_2 catalysts revealed by femtosecond diffuse reflectance spectroscopy. *The Journal of Physical Chemistry B, 103*, 3120–3127. https://doi.org/10.1021/jp984162h
50. Iwata, K., Takaya, T., Hamaguchi, H., Yamakata, A., Ishibashi, T., Onishi, H., & Kuroda, H. (2004). Carrier dynamics in TiO_2 and Pt/TiO_2 powders observed by femtosecond time-resolved near-infrared spectroscopy at a spectral region of 0.9–1.5 μm with the direct absorption method. *The Journal of Physical Chemistry B, 108*, 20233–20239. https://doi.org/10.1021/jp047531k
51. Schneider, J., & Bahnemann, D. (2018). Strong transient absorption of trapped holes in anatase and rutile TiO_2 at high laser intensities. *Journal of Physical Chemistry C, 122*, 13979–13985. https://doi.org/10.1021/acs.jpcc.8b01109
52. Kim, W., Tachikawa, T., Monllor-Satoca, D., Kim, H., Majima, T., & Choi, W. (2013). Promoting water photooxidation on transparent WO_3 thin films using an alumina overlayer. *Energy and Environmental Science, 6*, 3732–3739. https://doi.org/10.1039/c3ee42151a
53. Zhai, X.-P., Gao, L.-F., Zhang, H., Peng, Y., Zhang, X.-D., Wang, Q., & Zhang, H.-L. (2022). Defect engineering of ultrathin WO_3 nanosheets: Implications for nonlinear optoelectronic devices. *ACS Applied Nano Materials, 5*, 1169–1177. https://doi.org/10.1021/acsanm.1c03791
54. Sachs, M., Park, J.-S., Pastor, E., Kafizas, A., Wilson, A. A., Francàs, L., Gul, S., Ling, M., Blackman, C., Yano, J., et al. (2019). Effect of oxygen deficiency on the excited state kinetics of WO_3 and implications for photocatalysis. *Chemical Science, 10*, 5667–5677. https://doi.org/10.1039/C9SC00693A
55. Pesci, F. M., Cowan, A. J., Alexander, B. D., Durrant, J. R., & Klug, D. R. (2011). Charge carrier dynamics on mesoporous WO_3 during water splitting. *Journal of Physical Chemistry Letters, 2*, 1900–1903. https://doi.org/10.1021/jz200839n
56. Yang, Y., Forster, M., Ling, Y., Wang, G., Zhai, T., Tong, Y., Cowan, A. J., & Li, Y. (2016). Acid treatment enables suppression of electron-hole recombination in hematite for photoelectrochemical water splitting. *Angewandte Chemie International Edition, 55*, 3403–3407. https://doi.org/10.1002/anie.201510869
57. Pendlebury, S. R., Wang, X., Formal, F. L., Cornuz, M., Kafizas, A., Tilley, S. D., Grätzel, M., & Durrant, J. R. (2014). Ultrafast charge carrier recombination and trapping in hematite photoanodes under applied bias. *Journal of the American Chemical Society, 136*, 9854–9857. https://doi.org/10.1021/ja504473e
58. Pendlebury, S. R., Cowan, A. J., Barroso, M., Sivula, K., Ye, J., Grätzel, M., Klug, D. R., Tang, J., & Durrant, J. R. (2012). Correlating long-lived photogenerated hole populations with photocurrent densities in hematite water oxidation photoanodes. *Energy and Environmental Science, 5*, 6304. https://doi.org/10.1039/c1ee02567h
59. Fitzmorris, B. C., Patete, J. M., Smith, J., Mascorro, X., Adams, S., Wong, S. S., & Zhang, J. Z. (2013). Ultrafast transient absorption studies of hematite nanoparticles: The effect of particle shape on exciton dynamics. *Chemsuschem, 6*, 1907–1914. https://doi.org/10.1002/cssc.201300571
60. Pei, G. X., Wijten, J. H. J., & Weckhuysen, B. M. (2018). Probing the dynamics of photogenerated holes in doped hematite photoanodes for solar water splitting using transient absorption spectroscopy. *Physical Chemistry Chemical Physics: PCCP, 20*, 9806–9811. https://doi.org/10.1039/C8CP00981C
61. Pendlebury, S. R., Barroso, M., Cowan, A. J., Sivula, K., Tang, J., Grätzel, M., Klug, D., & Durrant, J. R. (2011). Dynamics of photogenerated holes in nanocrystalline α-Fe_2O_3 electrodes for water oxidation probed by transient absorption spectroscopy. *Chemical Communications, 47*, 716–718. https://doi.org/10.1039/C0CC03627G
62. Barroso, M., Cowan, A. J., Pendlebury, S. R., Grätzel, M., Klug, D. R., & Durrant, J. R. (2011). The role of cobalt phosphate in

enhancing the photocatalytic activity of α-Fe_2O_3 toward water oxidation. *Journal of the American Chemical Society, 133*, 14868–14871. https://doi.org/10.1021/ja205325v
63. Barroso, M., Pendlebury, S. R., Cowan, A. J., & Durrant, J. R. (2013). Charge carrier trapping, recombination and transfer in hematite (α-Fe_2O_3) water splitting photoanodes. *Chemical Science, 4*, 2724. https://doi.org/10.1039/c3sc50496d
64. Kamat, P. V., & Patrick, B. (1992). Photophysics and photochemistry of quantized ZnO colloids. *Journal of Physical Chemistry, 96*, 6829–6834. https://doi.org/10.1021/j100195a055
65. Bauer, C., Boschloo, G., Mukhtar, E., & Hagfeldt, A. (2004). Ultrafast relaxation dynamics of charge carriers relaxation in ZnO nanocrystalline thin films. *Chemical Physics Letters, 387*, 176–181. https://doi.org/10.1016/j.cplett.2004.01.106
66. Pastor, E., Pesci, F. M., Reynal, A., Handoko, A. D., Guo, M., An, X., Cowan, A. J., Klug, D. R., Durrant, J. R., & Tang, J. (2014). Interfacial charge separation in Cu_2O/RuO_x as a visible light driven CO_2 reduction catalyst. *Physical Chemistry Chemical Physics: PCCP, 16*, 5922–5926. https://doi.org/10.1039/C4CP00102H
67. Aiga, N., Jia, Q., Watanabe, K., Kudo, A., Sugimoto, T., & Matsumoto, Y. (2013). Electron−phonon coupling dynamics at oxygen evolution sites of visible-light-driven photocatalyst: Bismuth Vanadate. *Journal of Physical Chemistry C, 117*, 9881–9886. https://doi.org/10.1021/jp4013027
68. Kahraman, A., Barzgar Vishlaghi, M., Baylam, I., Sennaroglu, A., & Kaya, S. (2019). Roles of charge carriers in the excited state dynamics of $BiVO_4$ photoanodes. *Journal of Physical Chemistry C, 123*, 28576–28583. https://doi.org/10.1021/acs.jpcc.9b07391
69. Ravensbergen, J., Abdi, F. F., van Santen, J. H., Frese, R. N., Dam, B., van de Krol, R., & Kennis, J. T. M. (2014). Unraveling the carrier dynamics of $BiVO_4$: A femtosecond to microsecond transient absorption study. *Journal of Physical Chemistry C, 118*, 27793–27800. https://doi.org/10.1021/jp509930s
70. Kafizas, A., Xing, X., Selim, S., Mesa, C. A., Ma, Y., Burgess, C., McLachlan, M. A., & Durrant, J. R. (2019). Ultra-thin Al_2O_3 coatings on $BiVO_4$ photoanodes: Impact on performance and charge carrier dynamics. *Catalysis Today, 321–322*, 59–66. https://doi.org/10.1016/j.cattod.2017.11.014
71. Suzuki, Y., Murthy, D. H. K., Matsuzaki, H., Furube, A., Wang, Q., Hisatomi, T., Domen, K., & Seki, K. (2017). Rational Interpretation of correlated kinetics of mobile and trapped charge carriers: Analysis of ultrafast carrier dynamics in $BiVO_4$. *Journal of Physical Chemistry C, 121*, 19044–19052. https://doi.org/10.1021/acs.jpcc.7b05574
72. Miyasato, R., Fujiwara, M., Uragami, C., Sato, H., Yano, T., & Hashimoto, H. (2020). Operando time-resolved diffuse reflection spectroscopy: The origins of photocatalytic water-oxidation activity of Bismuth Vanadate. *Journal of Photochemistry and Photobiology, A: Chemistry, 395*, 112493. https://doi.org/10.1016/j.jphotochem.2020.112493
73. Okuno, K., Kumagai, H., Vequizo, J. J. M., Kato, K., Kobayashi, M., Yamakata, A., Kakihana, M., & Kato, H. (2022). Influences of pulverization and annealing treatment on the photocatalytic activity of $BiVO_4$ for oxygen evolution. *Sustainable Energy and Fuels, 6*, 1698–1707. https://doi.org/10.1039/D2SE00065B
74. Yamada, Y., Nakamura, T., Yasui, S., Funakubo, H., & Kanemitsu, Y. (2014). Measurement of transient photoabsorption and photocurrent of $BiFeO_3$ thin films: Evidence for long-lived trapped photocarriers. *Physical Review B, 89*, 035133. https://doi.org/10.1103/PhysRevB.89.035133
75. Li, Y., Adamo, C., Rowland, C. E., Schaller, R. D., Schlom, D. G., & Walko, D. A. (2018). Nanoscale excitonic photovoltaic mechanism in ferroelectric $BiFeO_3$ thin films. *APL Materials, 6*, 84905. https://doi.org/10.1063/1.5030628
76. Yamakata, A., Vequizo, J. J. M., & Kawaguchi, M. (2015). Behavior and energy state of photogenerated charge carriers in single-crystalline and polycrystalline powder $SrTiO_3$ studied by time-resolved absorption spectroscopy in the visible to mid-infrared region. *Journal of Physical Chemistry C, 119*, 1880–1885. https://doi.org/10.1021/jp510647b
77. Yamakata, A., Yeilin, H., Kawaguchi, M., Hisatomi, T., Kubota, J., Sakata, Y., & Domen, K. (2015). Morphology-sensitive trapping states of photogenerated charge carriers on $SrTiO_3$ particles studied by time-resolved visible to mid-IR absorption spectroscopy: The effects of molten salt flux treatments. *Journal of Photochemistry and Photobiology, A: Chemistry, 313*, 168–175. https://doi.org/10.1016/j.jphotochem.2015.05.016
78. Millers, D., Grigorjeva, L., Pankratov, V., Trepakov, V. A., & Kapphan, S. E. (2002). Pulsed electron beam excited transient absorption in $SrTiO_3$. *Nuclear Instruments and Methods in Physics Research Section B: Beam Interactions with Materials and Atoms, 194*, 469–473. https://doi.org/10.1016/S0168-583X(02)00951-5
79. Kamat, P. V., Dimitrijevic, N. M., & Fessenden, R. W. (1987). Photoelectrochemistry in particulate systems. 6. Electron-transfer reactions of small CdS colloids in acetonitrile. *The Journal of Physical Chemistry A, 91*, 396–401. https://doi.org/10.1021/j100286a029
80. Kamat, P. V., Ebbesen, T. W., Dimitrijević, N. M., & Nozik, A. J. (1989). Primary photochemical events in CdS semiconductor colloids as probed by picosecond laser flash photolysis. *Chemical Physics Letters, 157*, 384–389. https://doi.org/10.1016/0009-2614(89)87267-7
81. Uchihara, T., & Fox, M. A. (1996). Nanosecond laser flash photolysis of thiophenolate-capped cadmium sulfide particles in acetonitrile. *Inorganica Chimica Acta, 242*, 253–259. https://doi.org/10.1016/0020-1693(96)04875-X
82. Uchihara, T., Oshiro, H., & Kinjo, A. (1998). Subpicosecond studies of primary photochemical events of CdS particles with surface modified by various capping agents. *Journal of Photochemistry and Photobiology, A: Chemistry, 114*, 227–234. https://doi.org/10.1016/S1010-6030(98)00225-1
83. Wang, W., Tao, Y., Fan, J., Yan, Z., Shang, H., Phillips, D. L., Chen, M., & Li, G. (2022). Fullerene-graphene acceptor drives ultrafast carrier dynamics for sustainable CdS photocatalytic hydrogen evolution. *Advanced Functional Materials, 32*, 2201357. https://doi.org/10.1002/adfm.202201357
84. McArthur, E. A., Morris-Cohen, A. J., Knowles, K. E., & Weiss, E. A. (2010). Charge carrier resolved relaxation of the first excitonic state in CdSe quantum dots probed with near-infrared transient absorption spectroscopy. *The Journal of Physical Chemistry B, 114*, 14514–14520. https://doi.org/10.1021/jp102101f
85. Klimov, V. I., Schwarz, C. J., McBranch, D. W., Leatherdale, C. A., & Bawendi, M. G. (1999). Ultrafast dynamics of inter- and intraband transitions in semiconductor nanocrystals: Implications for quantum-dot lasers. *Physical Review B, 60*, R2177–R2180. https://doi.org/10.1103/PhysRevB.60.R2177
86. Khan, M. A., Maity, P., Al-Oufi, M., Al-Howaish, I. K., & Idriss, H. (2018). Electron transfer of the metal/semiconductor system in photocatalysis. *Journal of Physical Chemistry C, 122*, 16779–16787. https://doi.org/10.1021/acs.jpcc.8b03741
87. Corp, K. L., & Schlenker, C. W. (2017). ultrafast spectroscopy reveals electron-transfer cascade that improves hydrogen evolution with carbon nitride photocatalysts. *Journal of the American Chemical Society, 139*, 7904–7912. https://doi.org/10.1021/jacs.7b02869

88. Godin, R., Wang, Y., Zwijnenburg, M. A., Tang, J., & Durrant, J. R. (2017). Time-resolved spectroscopic investigation of charge trapping in carbon nitrides photocatalysts for hydrogen generation. *Journal of the American Chemical Society, 139*, 5216–5224. https://doi.org/10.1021/jacs.7b01547
89. Ye, C., Li, J.-X., Li, Z.-J., Li, X.-B., Fan, X.-B., Zhang, L.-P., Chen, B., Tung, C.-H., & Wu, L.-Z. (2015). Enhanced driving force and charge separation efficiency of protonated G-C_3N_4 for photocatalytic O_2 evolution. *ACS Catalysis, 5*, 6973–6979. https://doi.org/10.1021/acscatal.5b02185
90. Berger, T., Sterrer, M., Diwald, O., Knözinger, E., Panayotov, D., Thompson, T. L., & Yates, J. T. (2005). Light-induced charge separation in anatase TiO_2 particles. *The Journal of Physical Chemistry B, 109*, 6061–6068. https://doi.org/10.1021/jp044293
91. Al-Madanat, O., Nunes, B. N., AlSalka, Y., Hakki, A., Curti, M., Patrocinio, A. O. T., & Bahnemann, D. W. (2021). Application of EPR spectroscopy in TiO_2 and Nb_2O_5 photocatalysis. *Catalysts*. https://doi.org/10.3390/catal11121514
92. Berger, T., & Diwald, O. (2016). *Photocatalysis: Fundamentals and perspectives* (pp. 185–217). The Royal Society of Chemistry. https://doi.org/10.1039/9781782622338-00185 ISBN: 978-1-78262-041-9.
93. Zhang, Z., & Yates, J. T. (2010). Electron-mediated CO oxidation on the TiO_2(110) surface during electronic excitation. *Journal of the American Chemical Society, 132*, 12804–12807. https://doi.org/10.1021/ja106207w
94. Iorio, Y. D., Aguirre, M. E., Brusa, M. A., & Grela, M. A. (2012). Surface chemistry determines electron storage capabilities in alcoholic sols of titanium dioxide nanoparticles. A combined FTIR and room temperature EPR investigation. *The Journal of Physical Chemistry C, 116*, 9646–9652. https://doi.org/10.1021/jp301659t
95. Biswas, S., Husek, J., Londo, S., & Baker, L. R. (2018). Ultrafast electron trapping and defect-mediated recombination in NiO probed by femtosecond extreme ultraviolet reflection-absorption spectroscopy. *Journal of Physical Chemistry Letters, 9*, 5047–5054. https://doi.org/10.1021/acs.jpclett.8b01865
96. Henderson, M. A. (2011). A surface science perspective on TiO_2 photocatalysis. *Surface Science Reports, 66*, 185–297. https://doi.org/10.1016/j.surfrep.2011.01.001
97. Nunzi, F., Angelis, F. D., & Selloni, A. (2016). Ab initio simulation of the absorption spectra of photoexcited carriers in TiO_2 nanoparticles. *The Journal of Physical Chemistry Letters, 7*, 3597–3602. https://doi.org/10.1021/acs.jpclett.6b01517
98. Lawless, D., Serpone, N., & Meisel, D. (1991). Role of hydroxyl radicals and trapped holes in photocatalysis. A pulse radiolysis study. *The Journal of Physical Chemistry A, 95*, 5166–5170. https://doi.org/10.1021/j100166a047
99. Katoh, R., Murai, M., & Furube, A. (2010). Transient absorption spectra of nanocrystalline TiO_2 films at high excitation density. *Chemical Physics Letters, 500*, 309–312. https://doi.org/10.1016/j.cplett.2010.10.045
100. Smolin, S. Y., Choquette, A. K., Wang, J., May, S. J., & Baxter, J. B. (2018). Distinguishing thermal and electronic effects in ultrafast optical spectroscopy using oxide heterostructures. *Journal of Physical Chemistry C, 122*, 115–123. https://doi.org/10.1021/acs.jpcc.7b09592
101. Schneider, J., Nikitin, K., Dillert, R., & Bahnemann, D. W. (2017). Laser-flash-photolysis-spectroscopy: A nondestructive method? *Faraday Discussions, 197*, 505–516. https://doi.org/10.1039/C6FD00193A
102. Mocatta, D., Cohen, G., Schattner, J., Millo, O., Rabani, E., & Banin, U. (2011). Heavily doped semiconductor nanocrystal quantum dots. *Science (80-), 332*, 77–81. https://doi.org/10.1126/science.1196321
103. Zhou, S., Pi, X., Ni, Z., Ding, Y., Jiang, Y., Jin, C., Delerue, C., Yang, D., & Nozaki, T. (2015). Comparative study on the localized surface plasmon resonance of boron- and phosphorus-doped silicon nanocrystals. *ACS Nano, 9*, 378–386. https://doi.org/10.1021/nn505416r
104. Luther, J. M., Jain, P. K., Ewers, T., & Alivisatos, A. P. (2011). Localized surface plasmon resonances arising from free carriers in doped quantum dots. *Nature Materials, 10*, 361–366. https://doi.org/10.1038/nmat3004
105. Dorfs, D., Härtling, T., Miszta, K., Bigall, N. C., Kim, M. R., Genovese, A., Falqui, A., Povia, M., & Manna, L. (2011). Reversible tunability of the near-infrared valence band plasmon resonance in $Cu_{2-x}Se$ nanocrystals. *Journal of the American Chemical Society, 133*, 11175–11180. https://doi.org/10.1021/ja2016284
106. Agrawal, A., Cho, S. H., Zandi, O., Ghosh, S., Johns, R. W., & Milliron, D. J. (2018). Localized surface plasmon resonance in semiconductor nanocrystals. *Chemical Reviews, 118*, 3121–3207. https://doi.org/10.1021/acs.chemrev.7b00613
107. Li, Y., Wen, M., Wang, Y., Tian, G., Wang, C., & Zhao, J. (2021). Plasmonic hot electrons from oxygen vacancies for infrared light-driven catalytic CO_2 reduction on Bi_2O_{3-x}. *Angewandte Chemie International Edition, 60*, 910–916. https://doi.org/10.1002/anie.202010156
108. Cheng, H., Kamegawa, T., Mori, K., & Yamashita, H. (2014). Surfactant-free nonaqueous synthesis of plasmonic molybdenum oxide nanosheets with enhanced catalytic activity for hydrogen generation from ammonia borane under visible light. *Angewandte Chemie International Edition, 53*, 2910–2914. https://doi.org/10.1002/anie.201309759
109. Zhou, D., Li, X., Zhou, Q., & Zhu, H. (2020). Infrared driven hot electron generation and transfer from non-noble metal plasmonic nanocrystals. *Nature Communications, 11*, 2944. https://doi.org/10.1038/s41467-020-16833-1
110. Zhang, Z., Jiang, X., Liu, B., Guo, L., Lu, N., Wang, L., Huang, J., Liu, K., & Dong, B. (2018). IR-driven ultrafast transfer of plasmonic hot electrons in nonmetallic branched heterostructures for enhanced H_2 generation. *Advanced Materials, 30*, 1705221. https://doi.org/10.1002/adma.201705221
111. Lian, Z., Sakamoto, M., Vequizo, J. J. M., Ranasinghe, C. S. K., Yamakata, A., Nagai, T., Kimoto, K., Kobayashi, Y., Tamai, N., & Teranishi, T. (2019). Plasmonic p–n junction for infrared light to chemical energy conversion. *Journal of the American Chemical Society, 141*, 2446–2450. https://doi.org/10.1021/jacs.8b11544
112. Yang, W., Liu, Y., Cullen, D. A., McBride, J. R., & Lian, T. (2021). Harvesting sub-bandgap IR photons by photothermionic hot electron transfer in a plasmonic p–n junction. *Nano Letters, 21*, 4036–4043. https://doi.org/10.1021/acs.nanolett.1c00932
113. Lian, Z., Sakamoto, M., Matsunaga, H., Vequizo, J. J. M., Yamakata, A., Haruta, M., Kurata, H., Ota, W., Sato, T., & Teranishi, T. (2018). Near infrared light induced plasmonic hot hole transfer at a nano-heterointerface. *Nature Communications, 9*, 2314. https://doi.org/10.1038/s41467-018-04630-w
114. Yang, W., Liu, Y., McBride, J. R., & Lian, T. (2021). Ultrafast and long-lived transient heating of surface adsorbates on plasmonic semiconductor nanocrystals. *Nano Letters, 21*, 453–461. https://doi.org/10.1021/acs.nanolett.0c03911
115. Günnemann, C., Curti, M., Schneider, J., & Bahnemann, D. W. (2020). *Photochemistry* (Vol. 47, pp. 122–158). Royal Society of Chemistry. https://doi.org/10.1039/9781788016520-00122 ISBN: 9781788015547.
116. Schneider, J., Matsuoka, M., Takeuchi, M., Zhang, J., Horiuchi, Y., Anpo, M., & Bahnemann, D. W. (2014). Understanding TiO_2

photocatalysis: Mechanisms and materials. *Chemical Reviews, 114*, 9919–9986. https://doi.org/10.1021/cr5001892
117. Loeb, S. K., Alvarez, P. J. J., Brame, J. A., Cates, E. L., Choi, W., Crittenden, J., Dionysiou, D. D., Li, Q., Li-Puma, G., Quan, X., et al. (2019). The technology horizon for photocatalytic water treatment: Sunrise or sunset? *Environmental Science and Technology, 53*, 2937–2947. https://doi.org/10.1021/acs.est.8b05041
118. Colombo, D. P., & Bowman, R. M. (1995). Femtosecond diffuse reflectance spectroscopy of TiO_2 powders. *Journal of Physical Chemistry, 99*, 11752–11756. https://doi.org/10.1021/j100030a020
119. Katoh, R., Murai, M., & Furube, A. (2008). Electron–hole recombination in the bulk of a rutile TiO_2 single crystal studied by sub-nanosecond transient absorption spectroscopy. *Chemical Physics Letters, 461*, 238–241. https://doi.org/10.1016/j.cplett.2008.07.021
120. Furube, A., Shiozawa, T., Ishikawa, A., Wada, A., Domen, K., & Hirose, C. (2002). Femtosecond transient absorption spectroscopy on photocatalysts: $K_4Nb_6O_{17}$ and $Ru(bpy)_3^{2+}$-intercalated $K_4Nb_6O_{17}$ thin films. *The Journal of Physical Chemistry B, 106*, 3065–3072. https://doi.org/10.1021/jp011083o
121. Grela, M. A., & Colussi, A. J. (1996). Kinetics of stochastic charge transfer and recombination events in semiconductor colloids. Relevance to photocatalysis efficiency. *The Journal of Physical Chemistry A, 100*, 18214–18221. https://doi.org/10.1021/jp961936q
122. Kopelman, R. (1988). Fractal reaction kinetics. *Science (80-), 241*, 1620–1626. https://doi.org/10.1126/science.241.4873.1620
123. Plonka, A., Berlin, Y. A., & Chekunaev, N. I. (1989). Dispersive recombination in condensed phases. *Chemical Physics Letters, 158*, 380–382. https://doi.org/10.1016/0009-2614(89)87355-5
124. Kohlrausch, R. (1854). Theorie Des Elektrischen Rückstandes in Der Leidener Flasche. *Annalen Der Physik Und Chemie, 167*, 179–214. https://doi.org/10.1002/andp.18541670203
125. Williams, G., & Watts, D. C. (1970). Non-symmetrical dielectric relaxation behaviour arising from a simple empirical decay function. *Transactions of the Faraday Society, 66*, 80. https://doi.org/10.1039/tf9706600080
126. McNeil, I. J., Ashford, D. L., Luo, H., & Fecko, C. J. (2012). Power-law kinetics in the photoluminescence of dye-sensitized nanoparticle films: Implications for electron injection and charge transport. *Journal of Physical Chemistry C, 116*, 15888–15899. https://doi.org/10.1021/jp3030717
127. Albery, W. J., Bartlett, P. N., Wilde, C. P., & Darwent, J. R. (1985). A general model for dispersed kinetics in heterogeneous systems. *Journal of the American Chemical Society, 107*, 1854–1858. https://doi.org/10.1021/ja00293a008
128. Sieland, F., Schneider, J., & Bahnemann, D. W. (2017). Fractal charge carrier kinetics in TiO_2. *Journal of Physical Chemistry C, 121*, 24282–24291. https://doi.org/10.1021/acs.jpcc.7b07087
129. Plonka, A. (1988). Chapter 3. Dispersive kinetics in condensed phases. *Annual Reports Section "C" (Physical Chemistry), 85*, 47. https://doi.org/10.1039/pc9888500047
130. Nelson, J., Haque, S. A., Klug, D. R., & Durrant, J. R. (2001). Trap-limited recombination in dye-sensitized nanocrystalline metal oxide electrodes. *Physical Review B, 63*, 205321. https://doi.org/10.1103/PhysRevB.63.205321
131. Barzykin, A. V., & Tachiya, M. (2002). Mechanism of charge recombination in dye-sensitized nanocrystalline semiconductors: Random flight model. *The Journal of Physical Chemistry B, 106*, 4356–4363. https://doi.org/10.1021/jp012957+
132. Tamaki, Y., Furube, A., Murai, M., Hara, K., Katoh, R., & Tachiya, M. (2007). Dynamics of efficient electron–hole separation in TiO_2 nanoparticles revealed by femtosecond transient absorption spectroscopy under the weak-excitation condition. *Physical Chemistry Chemical Physics: PCCP, 9*, 1453–1460. https://doi.org/10.1039/B617552J
133. Levine, I. N. (2008). *Physical chemistry* (6th ed.). McGraw-Hill. ISBN: 9780072538625.
134. Zhang, J. Z., O'Neil, R. H., Roberti, T. W., McGowen, J. L., & Evans, J. E. (1994). Femtosecond studies of trapped electrons at the liquid—solid interface of aqueous CdS colloids. *Chemical Physics Letters, 218*, 479–484. https://doi.org/10.1016/0009-2614(94)00031-X
135. Horikoshi, S., Tsutsumi, H., Matsuzaki, H., Furube, A., Emeline, A. V., & Serpone, N. (2015). In situ picosecond transient diffuse reflectance spectroscopy of opaque TiO_2 systems under microwave irradiation and influence of oxygen vacancies on the UV-driven/microwave-assisted TiO_2 photocatalysis. *Journal of Materials Chemistry C, 3*, 5958–5969. https://doi.org/10.1039/C4TC02748E
136. AlSalka, Y., Hakki, A., Schneider, J., & Bahnemann, D. W. (2018). Co-catalyst-free photocatalytic hydrogen evolution on TiO_2: Synthesis of optimized photocatalyst through statistical material science. *Applied Catalysis B: Environmental, 238*, 422–433. https://doi.org/10.1016/j.apcatb.2018.07.045
137. Siebrand, W., & Wildman, T. A. (1986). Dispersive kinetics: A structural approach to nonexponential processes in disordered media. *Accounts of Chemical Research, 19*, 238–243. https://doi.org/10.1021/ar00128a002
138. Elton, D. C. (2018). Stretched exponential relaxation. https://doi.org/10.48550/arXiv.1808.00881.
139. Robel, I., Kuno, M., & Kamat, P. V. (2007). Size-dependent electron injection from excited CdSe quantum dots into TiO_2 nanoparticles. *Journal of the American Chemical Society, 129*, 4136–4137. https://doi.org/10.1021/ja070099a
140. Mongin, C., Moroz, P., Zamkov, M., & Castellano, F. N. (2018). Thermally activated delayed photoluminescence from pyrenyl-functionalized CdSe quantum dots. *Nature Chemistry, 10*, 225–230. https://doi.org/10.1038/nchem.2906
141. Draper, R. B., & Fox, M. A. (1990). Titanium dioxide photooxidation of thiocyanate: $(SCN)_2^-$ studied by diffuse reflectance flash photolysis. *Journal of Physical Chemistry, 94*, 4628–4634. https://doi.org/10.1021/j100374a048
142. Draper, R. B., & Fox, M. A. (1990). Titanium dioxide photosensitized reactions studied by diffuse reflectance flash photolysis in aqueous suspensions of TiO_2 powder. *Langmuir, 6*, 1396–1402. https://doi.org/10.1021/la00098a013
143. Tan, J. A., Rose, J. T., Cassidy, J. P., Rohatgi, S. K., & Wustholz, K. L. (2016). Dispersive electron-transfer kinetics of rhodamines on TiO_2: Impact of structure and driving force on single-molecule photophysics. *Journal of Physical Chemistry C, 120*, 20710–20720. https://doi.org/10.1021/acs.jpcc.6b01960
144. Peek, N. M., Jeffcoat, D. B., Moisii, C., van de Burgt, L., Profeta, S., Scott, S. L., & Stiegman, A. E. (2018). Reassessment of the electronic structure of Cr(VI) sites supported on amorphous silica and implications for Cr coordination number. *Journal of Physical Chemistry C, 122*, 4349–4358. https://doi.org/10.1021/acs.jpcc.7b12079
145. Yamakata, A., Ishibashi, T. A., & Onishi, H. (2001). Time-resolved infrared absorption spectroscopy of photogenerated electrons in platinized TiO_2 particles. *Chemical Physics Letters, 333*, 271–277. https://doi.org/10.1016/S0009-2614(00)01374-9
146. Sieland, F., Schneider, J., & Bahnemann, D. W. (2018). Photocatalytic activity and charge carrier dynamics of TiO_2 powders with a binary particle size distribution. *Physical Chemistry Chemical Physics: PCCP, 20*, 8119–8132. https://doi.org/10.1039/C8CP00398J
147. Tachiya, M., & Mozumder, A. (1975). Kinetics of geminate-ion recombination by electron tunnelling. *Chemical Physics Letters, 34*, 77–79. https://doi.org/10.1016/0009-2614(75)80204-1

148. Warman, J. M., De Haas, M. P., Pichat, P., & Serpone, N. (1991). Effect of isopropyl alcohol on the surface localization and recombination of conduction-band electrons in degussa P25 titania: A pulse-radiolysis time-resolved microwave conductivity study. *Journal of Physical Chemistry, 95*, 8858–8861. https://doi.org/10.1021/j100175a081
149. Anta, J. A. (2009). Random walk numerical simulation for solar cell applications. *Energy and Environmental Science, 2*, 387. https://doi.org/10.1039/b819979e
150. Nelson, J., & Chandler, R. E. (2004). Random walk models of charge transfer and transport in dye sensitized systems. *Coordination Chemistry Reviews, 248*, 1181–1194. https://doi.org/10.1016/j.ccr.2004.04.001
151. Austin, I. G., & Mott, N. F. (2001). Polarons in crystalline and non-crystalline materials. *Advances in Physics, 50*, 757–812. https://doi.org/10.1080/00018730110103249
152. Di Valentin, C., & Selloni, A. (2011). Bulk and surface polarons in photoexcited anatase TiO_2. *Journal of Physical Chemistry Letters, 2*, 2223–2228. https://doi.org/10.1021/jz2009874
153. Yang, S., Brant, A. T., Giles, N. C., & Halliburton, L. E. (2013). Intrinsic small polarons in rutile TiO_2. *Physical Review B, 87*, 125201. https://doi.org/10.1103/PhysRevB.87.125201
154. Balogh, Á., Lente, G., Kalmár, J., & Fábián, I. (2015). Reaction schemes that are easily confused with a reversible first-order reaction. *International Journal of Chemical Kinetics, 47*, 773–782. https://doi.org/10.1002/kin.20960
155. Tang, J., Durrant, J. R., & Klug, D. R. (2008). Mechanism of photocatalytic water splitting in TiO_2. Reaction of water with photoholes, importance of charge carrier dynamics, and evidence for four-hole chemistry. *Journal of the American Chemical Society, 130*, 13885–13891. https://doi.org/10.1021/ja8034637
156. Yamakata, A., Ishibashi, T. A., & Onishi, H. (2003). Kinetics of the photocatalytic water-splitting reaction on TiO_2 and Pt/TiO_2 studied by time-resolved infrared absorption spectroscopy. *Journal of Molecular Catalysis A: Chemical, 199*, 85–94. https://doi.org/10.1016/S1381-1169(03)00021-9
157. van Stokkum, I. H. M., Larsen, D. S., & van Grondelle, R. (2004). Global and target analysis of time-resolved spectra. *Biochimica et Biophysica Acta - Bioenergetics, 1657*, 82–104. https://doi.org/10.1016/j.bbabio.2004.04.011
158. Thibert, A., Frame, F. A., Busby, E., Holmes, M. A., Osterloh, F. E., & Larsen, D. S. (2011). Sequestering high-energy electrons to facilitate photocatalytic hydrogen generation in CdSe/CdS nanocrystals. *Journal of Physical Chemistry Letters, 2*, 2688–2694. https://doi.org/10.1021/jz2013193